Coarse-grained modeling of macromolecular solutions using a configuration-based approach

V. Venkataramani and R. Sureshkumar

Department of Energy, Environment, and Chemical Engineering, Washington University, Saint Louis, Missouri 63130

B. Khomami[a)]

Department of Chemical and Biomolecular Engineering, University of Tennessee, Knoxville, Tennessee 37996

(Received 9 January 2008; final revision received 30 June 2008)

Synopsis

An accurate, configuration-based, coarse-grained model for dilute macromolecular solutions is presented. The basic approach relies on exploring the macromolecular configurational diversity present in the flow of dilute polymeric solutions and identifying and partitioning the most frequently observed configurations, e.g., folds, half dumbbells, kinks, dumbbells, coils, and stretched states. The probability of finding any one of these configurations is calculated using a master configuration map that dictates the conditional probability of finding a configuration with a given chain extension. Each configuration class is modeled using a dumbbell description with a suitably modified drag coefficient. The configuration-based model is implemented using a Brownian dynamics simulation and the predictions are compared with the corresponding bead-spring model and finitely extensible nonlinear elastic dumbbell in homogeneous steady shear and uniaxial extension. Finally, prospects for model improvement are discussed. © *2008 The Society of Rheology.* [DOI: 10.1122/1.2964201]

I. INTRODUCTION

Modeling and simulation of the dynamics of synthetic and biopolymer solutions under flow are essential to process and product design in several technologies. Traditionally, the focus has been on describing macroscopic properties under flow conditions that are critical to applications such as polymer processing. Recently, the emergence of bio- and nanotechnologies have presented novel problems that require the description of flows at length scales comparable to molecular length scales and the accurate description of the diffusion of the center-of-mass of the molecules. Furthermore, they have enabled the study of dynamics at the single-molecule level thereby elucidating the diversity of events at this level. Molecular individuality is the crucial element in understanding the macroscopic dynamics of these macromolecular solutions. The fact that the evolution of molecules that exist in a variety of configurations at equilibrium is predisposed by their initial configuration and the nature of the flow field imposed diversifies the dynamics of indi-

[a)]Author to whom correspondence should be addressed; electronic mail: bkhomami@utk.edu

vidual molecules. Therefore, the key to developing models that accurately describe macroscopically observed properties lies in understanding the coupling between the evolution of the underlying microstructure and external force fields such as flow, thermal, or chemical gradients. While continuum-level models can provide semiquantitative description of the macroscopic viscoelastic stress, they do not attempt to capture the details of microstructure evolution. Brownian dynamics simulation (BDS), based on a realistic micromechanical description of the polymer chain (e.g. multisegment bead-spring models), can provide accurate information on the microstructure. However, self-consistent incorporation of BDS into a flow simulation can be computationally prohibitive or often infeasible for nonhomogeneous flows. Hence, it is desirable to develop computationally tractable multiscale simulations that contain sufficiently accurate microstructure information while capable of predicting the kinematics in nonhomogeneous flows. In this article, we present a hierarachical, configuration-based approach to the modeling of dilute polymer solutions under flow.

In the past decade, development of special purpose algorithms (e.g., combined finite element/Brownian dynamics method) together with the astounding increase in computational power have made possible process-level, concurrent multiscale flow simulations where stochastic differential equations for micromechanical models for polymer dynamics at the mesoscopic level are self-consistently solved together with the conservation equations for mass and momentum [Laso and Öttinger (1993); Hulsen *et al.* (1997); Somasi and Khomami (2000, 2001); Gigras and Khomami (2002); Suen *et al.* (2002); Lozinski *et al.* (2003); Gupta *et al.* (2004); Keunings (2004); Woo *et al.* (2004)]. Clearly, the accuracy of these multiscale simulations greatly depends on that of the mesoscopic-level model used to describe the polymer chain dynamics. Hence, much research effort in the past decades has been devoted to the development of accurate microstructural models for polymeric solutions as well as coarse graining approaches to allow efficient process level multiscale simulations of polymeric solutions [Bird *et al.* (1987a, 1987b); Hua *et al.* (1999); Öttinger (1999); Somasi *et al.* (2002); Underhill and Doyle (2004)].

Among the mesoscopic models, the bead-rod model presents the finest level of description for the macromolecule. The model is based on the concept of a Kuhn step, which determines the length of the rods in between beads, as the distance beyond which portions of the molecule execute uncorrelated motions. The bead-rod model has extensively been used to study the macroscopic response of the λ-DNA molecule by Hur *et al.* (2000). The model provides accurate predictions for both macroscopic properties such as the stresses and microstructural properties such as the distribution functions. However, for synthetic or biological polymers of interest, the use of the bead-rod model in complex flow calculations is impossible due to the large number of Kuhn steps required [$O(10^3)$]. At the next level of coarse graining is the bead-spring model which is obtained by replacing a set of rods with two beads connected by a phantom entropic spring. The beads represent the drag, while the springs mimic the concerted motion of the set of underlying bead-rod segments. The force-extension (FE) behavior of the spring is derived at equilibrium under the assumption that the internal degrees of freedom at scales finer than that represented by a spring have sufficient time to sample the configuration space accessible to them compared to the time scale of relaxation of the entire macromolecule, i.e., equilibriated local motions. Although the FE behavior of traditional models such as the Hookean or finitely extensible nonlinear elastic (FENE) model is valid only at equilibrium, the internal degrees of freedom account for sufficient configurational detail to provide reasonable predictions for both macroscopic and microscopic properties [Hur *et al.* (2000); Somasi *et al.* (2002); Schroeder *et al.* (2004); and references therein]. The use of the random walk spring model [Underhill and Doyle (2004, 2005)] at a finer scale of

description can exactly match the predictions of the bead-rod model with significant savings in time and computational cost [Venkataramani *et al.* (2008)]. Despite the accuracy and computational advantage of the bead-spring models, their incorporation into complex flow calculations is limited to a few springs [Koppol *et al.* (2007)]. Therefore, there is a need for coarse graining the description of the macromolecule further.

Dumbbell models are the favored choice for studying complex flows for two reasons. First, combining a Brownian dynamics approach with macroscopic flow equations is feasible, in terms of memory and computational requirements [Koppol *et al.* (2007)]. Second, dumbbell-based models can be simplified by approximating the configurational distribution function to, for instance, a Gaussian distribution, yielding constitutive models for the macroscopic stress. In the dumbbell model, the entire macromolecule is described as two beads connected by a spring. The configurational diversity of the underlying macromolecule is purely described by the elastic nature of the spring. Therefore, the spring force used to describe the molecule is crucial in order to obtain realistic predictions for macroscopic properties. The Oldroyd-B model {derived from the Hookean spring [Bird *et al.* (1987b)]} has been widely used to describe the behavior of Boger fluids, since it predicts a constant viscosity and a finite first normal stress coefficient. It has especially been successful in studying the stability of unidirectional shear-dominated flows [Sureshkumar and Beris (1995); Al-Mubaiyedh *et al.* (2000); Lin *et al.* (2004); Arora and Sureshkumar (2005)]. However, the Hookean spring extends infinitely, leading to unrealistic predictions for the extensional viscosity past the coil-to-stretch point. The FENE [Warner (1972)] model circumvents the problem of infinite extension by prescribing a maximum extension limit by making the spring force infinite as the spring approaches the maximum extension. The FENE model predicts a shear-thinning viscosity and first normal stress coefficient, as well as a plateau in the extensional viscosity at high extension rates [Herrchen and Öttinger (1997); Wiest and Tanner (1989)]. Moreover, the prediction of non-Newtonian phenomena of interest has led to its use in complex flow calculations, either via the CONNFESSIT method [Laso and Öttinger (1993); Öttinger *et al.* (1997)], or the LPM method [Halin *et al.* (1998)]. The FENE-P [Wedgewood and Bird (1988)] model, derived by applying the Peterlin approximation to the FENE model, has been widely used in complex flow studies {for e.g., in the analysis of turbulent drag reduction of dilute polymer solutions [Li *et al.* (2006)]} due to the ease of coupling with the governing equations of mass and momentum. However, in the FENE-P model, only the mean-squared end-to-end distance is constrained to be less than the squared maximum extension. This leads to quantitative differences between the predictions of the FENE and FENE-P models [Keunings (1997); Sizaire *et al.* (1999)]. Several modifications to the FENE-P model have been proposed to address this [van Heel *et al.* (1998)] and predict the stress-conformation hysteresis exhibited by polymer solutions in contraction-expansion flows using continuum-level constitutive equations derived from the FENE spring {for, e.g., FENE-L and FENE-LS [Lielens *et al.* (1998, 1999)], FENE-M, FENE-MR, FENE-LSM, and FENE-LSMR [Zhou and Akhavan (2004)]}. Although these models are improvements over the FENE-P model, they are complex to incorporate in a complex flow calculation, due to the increased number of equations required to describe the moments of the distribution function. Therefore, they have not been used as widely as the FENE-P model.

The inaccurate predictions of the FENE dumbbell models have been attributed to the lack of sufficient internal degrees of freedom required to faithfully describe the flow-induced changes in the configuration of the molecule. Doyle *et al.* (1998) proposed a configuration-dependent drag that varies linearly with the extension of the FENE dumbbell in order to account for the change in the drag experienced by the molecule as it

transitions from a coiled state to an extended state. In this case, the ratio of the maximum to coiled-state drag coefficient can be used as a parameter to obtain close agreement with experimental observations. The idea was extended by Schroeder *et al.* (2004) to incorporate the effect of hydrodynamic interactions (HI) through a conformation dependent drag calculated from BDSs. Multiple relaxation modes were incorporated in the FENE-PM model developed by Wedgewood *et al.* (1991) and the adaptive length scale (ALS) model developed by Ghosh *et al.* (2002). In the FENE-PM model, an approximation to the multimode FENE-P model leads to a decoupling and reduction in the number of equations for the stresses from the different modes. In the ALS model, the number of segments used to describe the molecule varies based on the strain experienced: close to equilibrium and at high extensions, a single dumbbell model is used, whereas at intermediate extensions, a number of internal segments are introduced to represent the complex configurations assumed by the molecule. The model predicts the tensile stress in good agreement with a bead-spring model, while providing only a qualitative prediction of the stress conformation hysteresis. However, under steady shear, the model still suffers deficiencies and predicts stresses which are comparable to those obtained from the FENE dumbbell model.

Coarse graining, as can be noted from the extensive research that has been undertaken to date, has met with several obstacles due to the inherent nature of its development, i.e., reducing the level of detail in order to save computational time. The loss of detail has always directly led to a loss in the accuracy of the predicted microscopic and macroscopic properties. Although the dumbbell description is favorable for implementation in a complex flow calculation due to the reduced degrees of freedom, the macroscopic properties predicted by the dumbbell models have been shown to be at best qualitative in comparison to experimental observations [Doyle *et al.* (1998)]. Based on the findings of single molecule studies, this deviation from observed properties is known to stem from the lack of configurational information in the description of the macromolecule [Perkins *et al.* (1997); Smith *et al.* (1999); Babcock *et al.* (2000, 2003); Doyle *et al.* (2000); Schroeder *et al.* (2003); Teixeira *et al.* (2005)]. However, coupling bead-spring models with complex flow calculations is still a challenge due to limitations of computation and memory. We seek to address this issue by constructing a configuration-based, coarse-grained model that incorporates configurational information by the partitioning of the phase space accessible to the molecule into a few configuration classes. We incorporate the configurational diversity of the molecule by describing the evolution of the distributions of these configuration classes under flow while each of these classes is described using a simple dumbbell model. We distinguish among dumbbells belonging to different configuration classes by evaluating specific properties that are characteristic of the configuration class.

The article is organized as follows. We begin by studying the configurational diversity of a macromolecule in two standard flow types, namely, shear and uniaxial extension to elucidate the importance of molecular individuality in Sec. II. We identify a few distinct classes into which most configurations can be classified and use these as a basis set to explore the configurational phase space of the macromolecule in Sec. III A. A dumbbell-based model is developed for each of the configuration classes by calculating a modified drag coefficient for each configuration class in Sec. III B. The procedure for the implementation of the configuration-based model using the two concepts developed in Secs. III A and III B is presented in Sec. III C followed by the predictions of the coarse-grained model in Sec. IV. Finally a discussion of the model along with prospects for improvement are presented in Sec. V.

II. CONFIGURATIONAL DIVERSITY

In this section, we investigate the configurational diversity of a macromolecule by studying the phase space sampled by the λ-DNA molecule under standard flow types, namely, steady shear, and uniaxial extension. Within the last decade, the use of video fluorescence microscopy has led to a tremendous amount of research on the DNA molecule, particularly its static and dynamic properties and behavior under different flow conditions [Perkins *et al.* (1997); Smith and Chu (1998); Smith *et al.* (1999)]. The λ-DNA molecule in varying lengths has increasingly been used due to its long chain nature that allows for easy visualization under the microscope. Tags can be attached at the ends of the molecule and it can be fluorescently dyed to track the dynamics. Several studies have also focused on modeling the DNA molecule using bead-rod and bead-spring descriptions and have provided excellent comparisons with experimental observations for both macroscopic and microscopic properties [Hur *et al.* (2000); Somasi *et al.* (2002)]. The model description for the molecule has also been well documented. Therefore, the λ-phage DNA molecule is considered in this study. The findings from the sampling of the phase space of the molecule are then used to elucidate the relevance of molecular individuality by relating the configurational distributions to observed macroscopic properties. The macromolecule is described as a set of beads connected by springs. We consider free-draining molecules in the absence of excluded-volume effects. The configurational diversity of the molecule is studied via the Brownian dynamics (BD) approach. In this method, around 10^3–10^4 identical model molecules (also referred to as trajectories) are assigned random initial configurations. The trajectories are equilibrated and then exposed to flow. We observe the configurations of each of these trajectories as they evolve under the influence of flow via an automated configuration sorting algorithm. Experiments by Smith and co-workers [Smith and Chu (1998); Smith *et al.* (1999)] showed the existence of several configuration types such as folds, half dumbbells, kinks, dumbbells, coils, and stretched in several different flow types. We use these configuration classes to classify the configurations sampled by the macromolecule. The details of the governing equations, model parameters, solution procedure, and configuration sorting are presented in the Appendix.

A. Steady shear flow

The velocity field in steady shear flow is given as $v_x = \dot{\gamma} y$, $v_y = v_z = 0$, where $\dot{\gamma}$ is the shear rate. The rotational and extensional components of the flow field are equal. This gives rise to very interesting dynamics, both at a configurational as well as macroscopic level.

Figure 1 shows the evolution of the shear [(a) τ_{xy}] stress, tensile [(b) τ_{xx}] stress and the configurational probabilities (c) as a function of time from the inception of steady shear flow at Wi = 10 and 100. Figures 1(a) and 1(b) clearly show the existence of an overshoot for the shear and tensile stresses respectively. At Wi = 10, the magnitude of the overshoot is not very large with respect to the steady state stress that is attained for both the shear and tensile stress. Accordingly, the configurational probability distributions (CPDs) do not exhibit overshoots. The CPDs monotonically increase to their steady state distributions for all configuration classes, except for the coiled configuration class. However, at higher Wi, the magnitude of the overshoot is larger for both the shear and tensile stresses. This is reflected in the corresponding overshoot in the CPD, especially for the folded and stretched states. The overshoot in the shear stress occurs due to an initial alignment and stretching of coiled configurations along the direction of flow [Babcock *et al.* (2000)] and is seen to coincide with a minimum in the coiled configuration state. The insets in Fig. 1

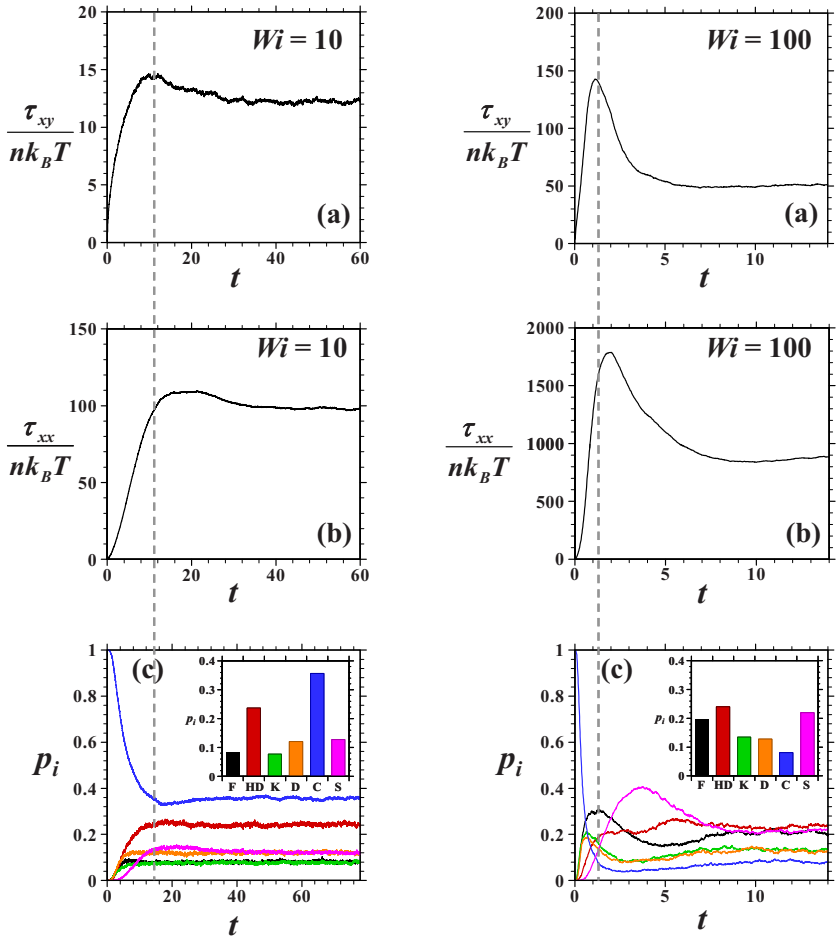

FIG. 1. Comparison of the (a) shear stress (τ_{xy}) scaled with (nk_BT), (b) tensile stress (τ_{xx}) scaled with (nk_BT), and (c) configurational probabilities (p_i) as a function of time for the λ-DNA molecule at Wi = 10 and 100. The insets in (c) show the steady state configurational probability distribution for each of the Wi.

show that the steady state CPD shows a discernable probability of occurrence for all the configuration classes, consistent with end-over-end tumbling dynamics [Smith *et al.* (1999); Doyle *et al.* (2000)]. Figure 2 shows the steady state CPD as a function of Wi and shows the existence of all the configuration classes even for large Wi. This can be explained by the fact that in shear flow at steady state, once a molecule is stretched out by flow, there is a finite probability that a Brownian fluctuation in the velocity gradient direction might be large enough to displace the molecule out of the shear direction and cause a tumbling event. As the molecule tumbles, it returns to a coiled state. Based on previous observations, depending on the initial coiled configuration of the molecule, its evolution can be different. Since the choice of the coiled configuration is random following tumbling, there is almost an equal probability of it evolving into any one of the five other configuration classes. At lower Wi we observe higher probabilities for the coiled state, which can be explained by analyzing the frequency of tumbling. It has been observed earlier by Teixeira *et al.* (2005) that the tumbling frequency scales with Wi to the power of 2/3. This implies that the rate of stretching of the molecule is slower at lower Wi than at larger Wi, thereby allowing the molecule to spend longer times in the coiled

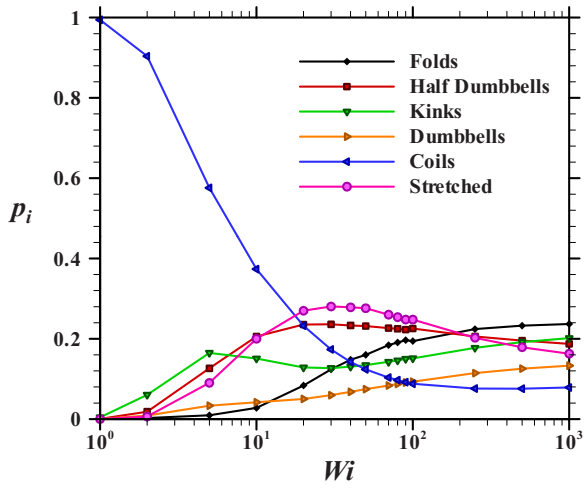

FIG. 2. Steady state configurational probability distributions, p_i, as a function of Wi for the different configuration classes under steady shear flow.

configuration. At higher Wi the molecule unravels quickly followed by a tumbling event, and then returns to the coiled state from where it can equally populate any of the configuration classes. Therefore, at very large Wi the steady state CPDs approach nearly a constant distribution.

B. Steady uniaxial extensional flow

The velocity field in uniaxial extensional flow is given as $v_x=\dot{\epsilon}x$, $v_y=-(\dot{\epsilon}/2)y$ and $v_z=-(\dot{\epsilon}/2)z$, where $\dot{\epsilon}$ is the extension rate. Extensional flows are different from shearing flow since the rates of extension and rotation are not the same. Therefore, there are differences in the dynamics at the microstructural level, leading to different steady state configurations and macroscopic properties [Perkins *et al.* (1997); Smith *et al.* (1999)].

Figure 3 shows the dimensionless elongational viscosity $[(\tau_{xx}-\tau_{yy})/\dot{\epsilon}]$ as a function of the Wi. The coil-to-stretch transition occurs around a dimensionless critical extension of Wi=0.5 [de Gennes (1974)]. At high Wi, the elongational viscosity plateaus to a new value much greater than three times the zero shear viscosity. Figure 4 shows a plot of the tensile stress and the corresponding CPDs as a function of time for Wi=0.5, 1, and 100. In Fig. 3, these are marked with black diamond symbols. Below the critical extension rate, the only configuration that exists is the coiled state. However, around Wi=0.5, we observe the occurrence of other configuration classes. At Wi=1, we continue to observe many configuration classes even at steady state, even though the flow is purely extensional. The existence of a bistable configuration region near the critical strain rate has already been proposed by de Gennes (1974) and proven by Schroeder *et al.* (2003). We support this finding further by calculating the CPDs at steady state near the critical extension rate. It can be seen that near Wi=0.5, more than one configuration class is probable, but at higher Wi the only configuration sampled is the stretched state, explaining the occurrence of a stress-conformation hysteresis. A plot of the steady state CPDs under uniaxial extensional flow as a function of Wi (Fig. 5) also displays the existence of multiple configuration classes in a narrow window around the critical strain rate. Stress-conformation hysteresis can further be understood by studying the configurational distributions that are observed upon the relaxation of molecules that were initially at steady

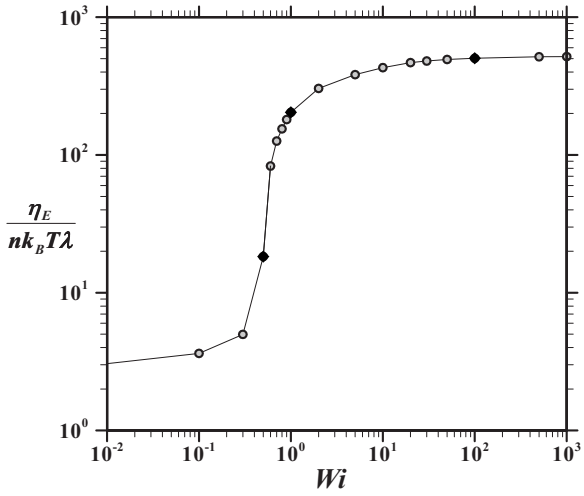

FIG. 3. Dimensionless elongational viscosity (η_E) scaled with ($nk_BT\lambda$) as a function of Wi for the λ-DNA molecule using a bead-spring description.

state under uniaxial elongational flow. The point at which the cessation of flow occurs is indicated by the line marker in Fig. 4. The configurational distribution functions are significantly different from those observed during the start-up, indicating that the pathway for relaxation of molecules is different from that during start-up. This further confirms the existence of hysteresis when comparing start-up with relaxation in extensional flows. The hysteresis can be explained based on the variable hydrodynamic drag that is exerted by the flow field on molecules with different configurations.

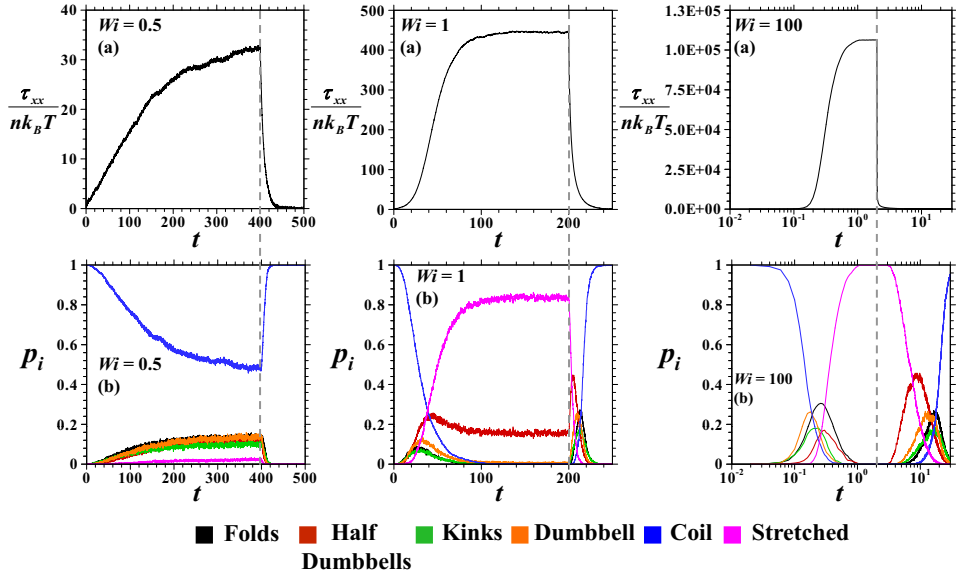

FIG. 4. Comparison of the (a) tensile stress, τ_{xx} scaled with (nk_BT) and (b) configurational probability distributions, p_i, as a function of time for Wi=0.5, 1, and 100. Note that the x axis for Wi=100 is on a log scale.

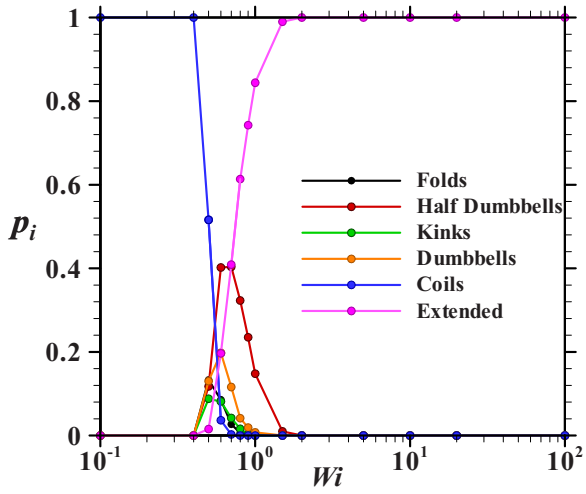

FIG. 5. Steady state configurational probability distributions (p_i) as a function of Wi under uniaxial extensional flow for the λ-DNA molecule using a bead-spring representation.

III. CONFIGURATION-BASED, COARSE-GRAINED MODEL

The existence of configurations that are ubiquitous in different flow types has provided a basis for the development of a coarse-grained model. These configuration classes can be viewed as subsets of the phase space of all accessible configurations such that at equilibrium only the coiled state is accessible while under flow conditions several other states are accessible. Each configuration class is a subset consisting of all molecules with a prescribed mesoscopic configuration; each class thereby has a distribution function that describes the diversity of configurations within the subset. For example, all molecules in a stretched state can be classified into a subset, and the associated distribution function describes the distribution of the lengths of the molecules that constitute this configuration class. The sum of the subsets will yield the total phase space. Therefore, the probability of occurrence p_i of a configuration class i can be calculated as a ratio of the partition function of the configuration class to that of the entire phase space. In a BDS, this can easily be calculated as a ratio of the number of trajectories of a given configuration N_i to the total number of trajectories N_T, i.e.,

$$p_i = \frac{N_i}{N_T}. \tag{1}$$

The description of a configuration class requires the calculation of the probability distribution function within the class and a measure of the frictional property of the configuration class in order to calculate the macroscopic stresses associated with the configuration class. These properties have been traditionally studied by analyzing the configurations at equilibrium and using statistical mechanics principles to relate them to coarse-grained properties. However, in the development of the configuration-based model, the existence of several of the classes only outside equilibrium has precluded the use of these standard procedures of statistical mechanics. Therefore, we seek other strategies to calculate these properties by studying the nonequilibrium configurations.

Instead of invoking approximations for the distribution function of configuration classes, we use BD simulations using detailed microstructural models to guide us in calculating distribution functions for the different configuration classes. Although the

macromolecule is coarse grained into a single dumbbell description, the hydrodynamic/elastic properties of the dumbbells of different configuration classes are not the same. We investigate different routes to effectively describe the properties of the different configuration classes by studying the hydrodynamic and elastic properties, and dynamical behavior of the configuration classes, using a fine-grained model. The development of the coarse-grained model based on configuration classes can therefore be broken down into two steps: (i) obtaining the distribution function within a configuration class, and (ii) developing a coarse-grained representation that is unique to each configuration class.

A. Configurational distribution functions

Using the coarse-grained description, the distribution function of molecules belonging to a particular configuration class must represent the underlying distribution of the fine-scaled description of the macromolecule. Since the macromolecule is coarse-grained into a single dumbbell, the quantity of interest is the end-to-end vector. The end-to-end vector is the simplest microstructural variable that can directly be derived as a vector sum of the orientation vectors of the springs of the underlying fine-scale model. This linear addition allows for a straightforward derivation of the equation that governs the evolution of the dumbbells. Therefore, while developing distribution functions for the different configuration classes, we are interested only in the distribution of the end-to-end vector. However, the task of calculating this distribution function is complicated by the fact that different flow fields have different effects on the mesoscopic configuration, leading to different distribution functions. Hence, a few key simplifications are made in order to make this a more tractable problem.

The two distinct variables in our description, namely, the configuration class and the end-to-end distance, are used to parametrize the phase space accessible to the molecules. If we focus on molecules with a chosen end-to-end distance Q, the partitioning of the phase space into six configuration classes dictates that the configuration of a molecule with the selected end-to-end distance must belong to one of the six configuration classes. Therefore, if the probability that a molecule with a given end-to-end distance belongs to one of the six configuration classes be written as $p(i|Q)$, such that

$$\sum_{i=1}^{N_{\text{conf}}} p(i|Q) = 1, \tag{2}$$

we can generate a configuration map of the conditional probabilities of the different configuration classes as a function of the end-to-end distance. In a BDS, $p(i|Q)$ can be calculated by counting the number of trajectories of a given configuration class (i) with a chosen end-to-end distance (Q) and dividing it by the total number of trajectories with the same end-to-end distance. Again, different flow fields and transients can lead to different calculated configuration maps. However, to provide a representation of all the different configuration maps, we hypothesize that the configuration map is not a strong function of the flow type or transients, and we generate a master configuration map (MCM) that is calculated as an average over many different flow types, flow strengths, and strains. Obviously, this simplification can lead to differences between the actual and calculated distribution functions, and the effect of the hypothesis will be put to test as described in the following sections. The MCM thus generated provides a measure of global transition probabilities between configuration classes in the form of a conditional probability of occurrence for a configuration type for a fixed end-to-end distance. This guides the evolution of the dumbbells as well as the configuration class they will fall under as they are strained by the flow. The use of the configuration map to calculate the configurational

distribution functions will be elaborated in Sec. III C which describes the implementation of the configuration-based model.

The calculation of the MCM requires a systematic exploration of the configuration classes sampled by the molecule as it is exposed to different flow types. Although this seems to be an intractable problem, for the purpose of generating the configuration map we choose only steady shear, steady uniaxial elongation, and steady biaxial elongation, and study the evolution of the configurations of the trajectories as a function of strain and that of flow strength. These three flow types are chosen since they span the region of allowable combinations of the invariants of the finger strain tensor [Bird *et al.* (1987a)]. Uniaxial extension and biaxial stretching are the boundaries of the invariant space, while simple shear is in the middle of the allowable region. Using the configurational distributions thus obtained, we can generate the MCM. Figures 6(a), 7(a), and 8(a) show representative plots of the CPDs as a function of time at Wi=100 in steady shear, biaxial extension, and uniaxial extension, respectively. The conditional probabilities for the different configuration classes for selected end-to-end distances (i.e., 25%, 50%, and 75% of the maximum stretch of the molecule) are, respectively, shown as a function of strain for the same flow strength in Figs. 6(b), 7(b), and 8(b). Under steady shear, the molecules initially transition from a coiled state into various configuration classes ($t=1.4$). At dimensionless times of 2.8 and 4.2, the stretched configuration has a higher probability of occurrence, coinciding with the overshoot in the shear and normal stresses. However, at steady state ($t=8.4$), most of the configurations are equally populated, which is in accord with the tumbling dynamics. From the plots for the conditional probability [Fig. 6(b)], it can be seen that molecules with an end-to-end distance equal to 25% of the maximum stretch favor the folded configuration, molecules with a fractional end-to-end distance of 0.5 favor the half dumbbell and kinked configurations, and molecules with a fractional end-to-end distance of 0.75 prefer the half dumbbell and stretched configurations.

In biaxial extensional flow [Fig. 7(a)], initially, the molecules are mostly coiled ($t=0.175$). As the strain ($t=0.35$) approaches the critical strain at which the coil-to-stretch transition occurs, most of the configuration classes are equally populated. However, past the critical strain, most of the molecules transition into a stretched state. This is consistent with the series of molecular events that occurs in extensional flows. A similar trend is also observed under uniaxial extension [Fig. 8(a)].

The plots for the conditional probability of occurrence of configuration classes are carefully analyzed in biaxial and uniaxial extensional flow. For strains greater than the critical strain, the configurational probability distributions clearly show that the molecules are predominantly in the stretched state. However, the conditional probability calculated for molecules with a fractional end-to-end distance of 0.25 shows that the folded state is the only configuration that these molecules sample. Based on the corresponding configurational distribution function, it can be clearly noted that the molecular population corresponding to a fractional end-to-end distance of 0.25 is very small. Therefore, the conditional probabilities calculated for this fractional end-to-end distance are biased, due to limitations posed by the BDS technique used to calculate the conditional probabilities. Therefore, when developing configuration maps, we consider only those conditional probability plots wherein the ensemble sizes are significantly large ($>10\%$ of the total ensemble size) to allow for the calculation of meaningful distributions. Typically, in extensional flows, conditional probabilities calculated are meaningful for most configuration classes only below the critical strain while at higher strains, conditional probabilities corresponding to the end-to-end distance of the stretched states can be easily calculated. Therefore, in the case of uniaxial extensional flow, in Fig. 8(b), we present the conditional probability distributions only below the critical extension rate.

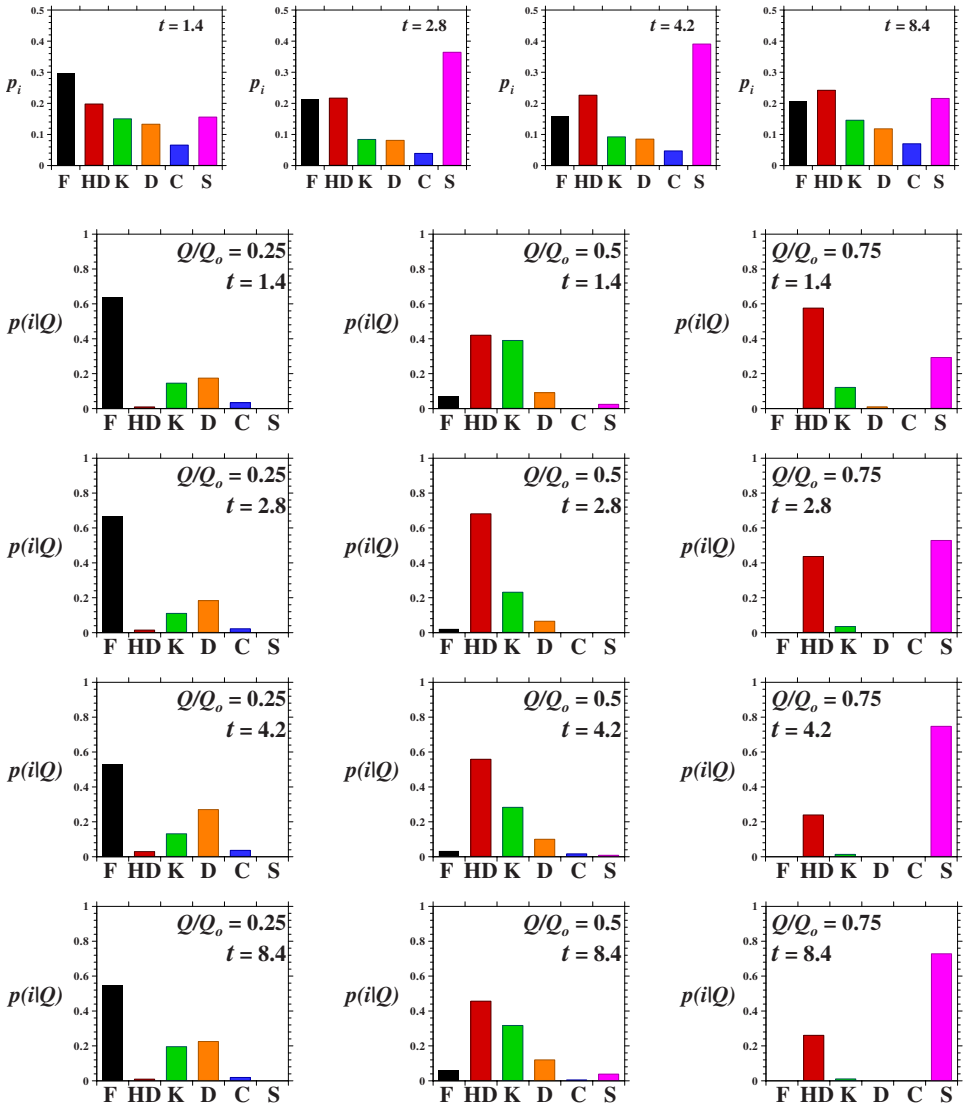

FIG. 6. (a) Configurational probability distributions as a function of time in steady shear flow at Wi=100. (b) Conditional probability distribution functions for the end-to-end distance of different configuration classes as a function of time under steady shear flow at Wi=100.

A persistent trend that can be observed by comparing Figs. 6(b), 7(b), and 8(b) is that for a fractional end-to-end distance of 0.25, the folded configuration is preferred, while for a fractional end-to-end distance of 0.5, half dumbbell and kinked configurations are preferred, and for a fractional end-to-end distance of 0.75, half dumbbell, kinked, and stretched states are preferred. Moreover, the probability of occurrence of any one of these configuration classes is approximately the same in all the conditional probability plots. This observation is independent of the flow type, strain or the individual configurational distribution functions that vary with different flow types. It therefore provides a basis to support the accuracy and applicability of the MCM hypothesis. Conditional probability plots similar to Figs. 6(b), 7(b), and 8(b) were computed for various Wi and at various

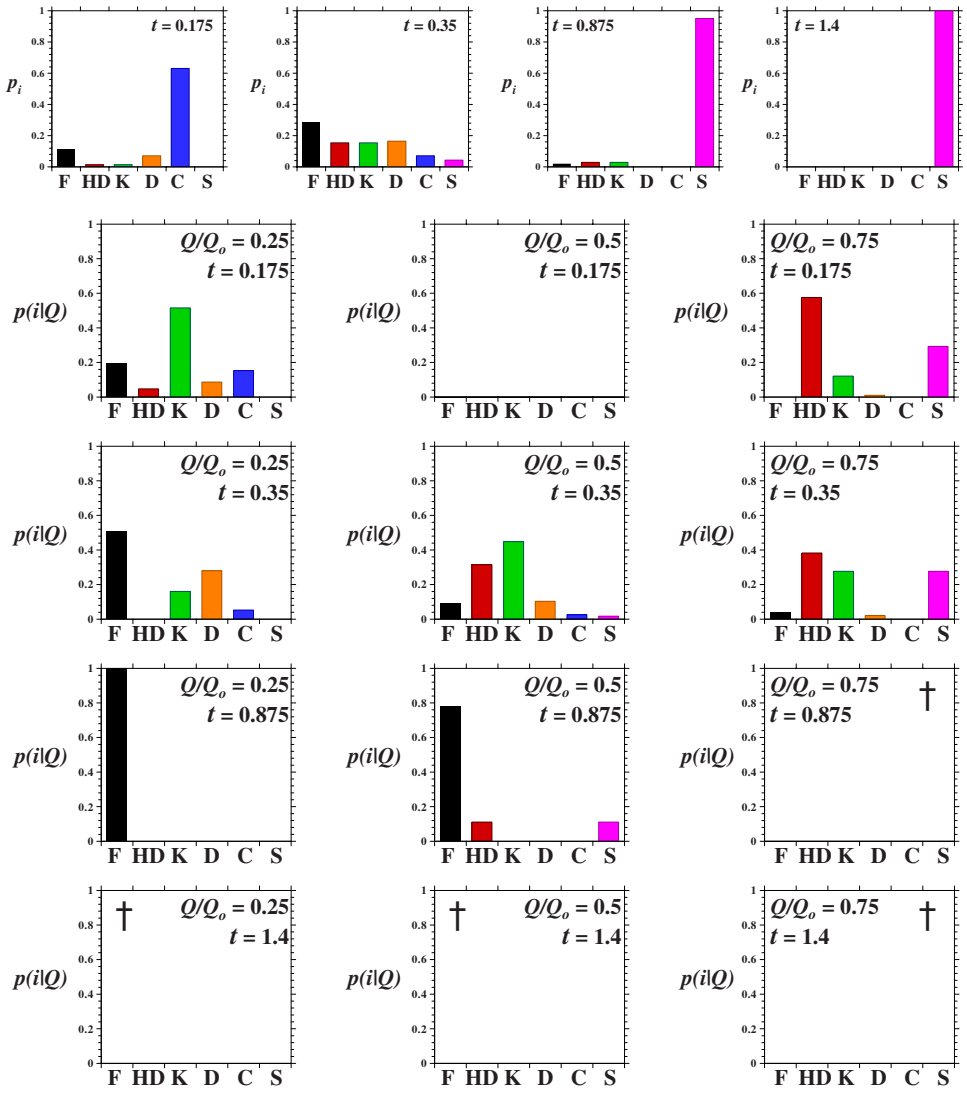

FIG. 7. (a) Configurational probability distributions as a function of time in steady biaxial extensional flow at Wi = 100. (b) Conditional probability distribution functions for the end-to-end distance of different configuration classes as a function of time under steady biaxial extensional flow at Wi = 100.† Note, there are no configurations present at these extensions under biaxial extension for Wi = 100.

strains. An average over all these different conditional probability plots yields the MCM. Here, we present a consolidated MCM wherein the conditional probability of a configuration is plotted along the abscissa and the corresponding end-to-end distance is plotted along the ordinate in Fig. 9. The conditional probability of a configuration class for a particular end-to-end distance can be calculated as the fractional length of the bar corresponding to the particular configuration class. Based on Eq. (2), the total length of each bar must be equal to unity.

B. Coarse-grained models for describing configuration classes

The second step in the development of the coarse-grained model is to obtain unique representations for the configuration classes, so that the dynamical properties of interest

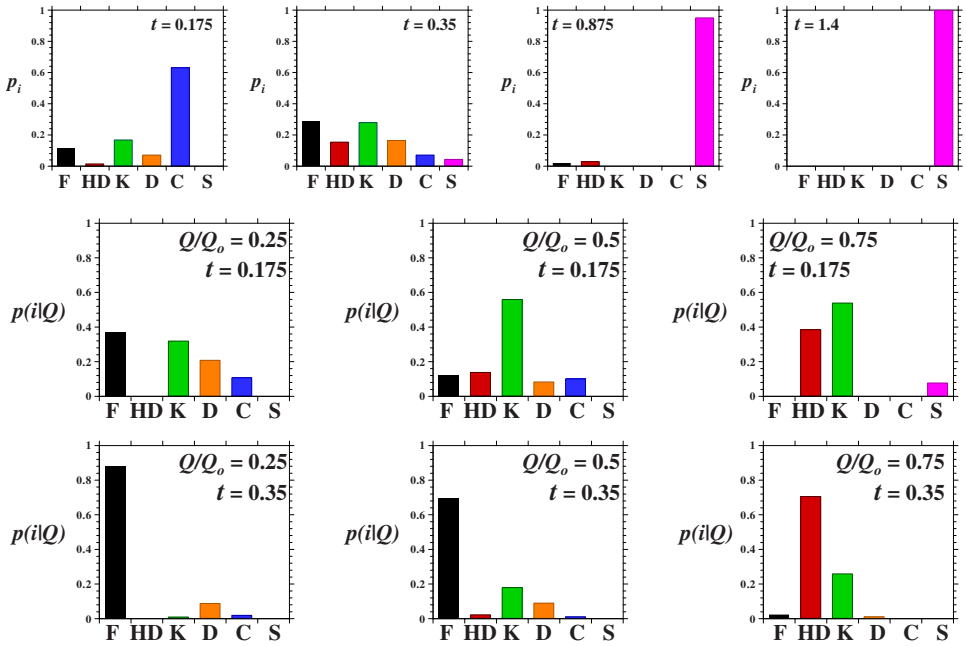

FIG. 8. (a) Configurational probability distributions as a function of time in steady uniaxial extensional flow at Wi = 100. (b) Conditional probability distribution functions for the end-to-end distance of different configuration classes as a function of time under steady uniaxial extensional flow at Wi = 100.

for the coarse-grained description are in agreement with the underlying fine-grained model. The coarse-grained dumbbell model experiences hydrodynamic drag forces on the beads and elastic forces from the spring. These drag and elastic forces offer routes to alter the properties of the coarse-grained model, and we investigate the effect of modifying

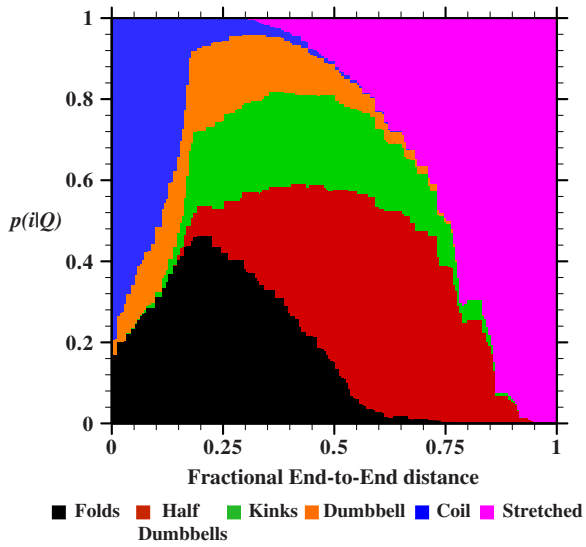

FIG. 9. Master configuration map showing the conditional probability of occurrence of different configuration classes as a function of the end-to-end distance.

them in the following sections. The modification of the hydrodynamic properties of the dumbbell can be incorporated via the drag coefficient of the bead or the relaxation time of the molecule. Since the relaxation time is indirectly related to the drag coefficient, modifying one of these properties will directly lead to a modification of the other. However, these two approaches will be studied independently in order to elucidate the advantage of using one over the other for estimating modified properties. The modification of the elastic properties, on the other hand, is incorporated via the calculation of a new elastic force that varies with the configuration class.

The modified hydrodynamic or elastic property of the coarse-grained dumbbell model is usually determined by equating it to the corresponding property calculated for a multibead spring model. A method often used to calculate properties of a coarse-grained representation is to simulate the constant extension ensemble. In this method, the ends of a molecule are held fixed at a chosen distance by applying an external force at one or both ends of the molecule and allowing it to evolve in either the presence or absence of flow. Elastic/drag properties can be evaluated by averaging the desired property over very large times to allow for an adequate sampling of the phase space. The technique has been used to calculate force laws as a function of the degree of coarse graining by Underhill and Doyle (2004; 2005) and for modified drag coefficients for systems in the presence of HI by Schroeder *et al.* (2004). It has also been shown that using the constant extension ensemble is the correct way to calculate coarse-grained properties, rather than using the constant force ensemble [Underhill and Doyle (2004)] since it predicts the same response as the true polymer under all constraints rather than one which is specific to the experiment used to calculate the coarse-grained property as in the constant-force ensemble. However, in the development of the configuration-based model, the use of the constant extension ensemble can pose constraints that complicate the calculation of elastic/hydrodynamic properties. The basis of the configuration based model is the existence of prominent configuration classes that have been previously identified. The constraints posed on the ends of the chain in the constant extension ensemble can therefore bias the configurations sampled by the molecule, thereby leading to the overpopulation of configuration classes in some cases, and to the exclusion of certain configuration classes entirely in other cases. Therefore, we seek to develop a similar methodology while allowing for the sampling of the configuration phase space of interest.

1. Drag coefficient

The concept of a modified drag coefficient for each configuration class is motivated by the fact that the drag force experienced by an object is directly related to its size and shape. For example, we know that the hydrodynamic drag force on a sphere translating in a fluid is different from that of a rod translating through the fluid. Similarly, the configurations that have been identified as the basis for the coarse-grained model can also be envisioned as different sized/shaped objects having differing drag properties when exposed to flow in solution. Therefore, when developing a coarse-grained model wherein different configuration classes are represented by the same physical representation (a dumbbell), a natural choice for incorporating the configurational diversity is the drag coefficient of the dumbbells based on the configuration class they represent.

For calculating a modified drag coefficient for each configuration class, it is required to fix the elastic properties of the molecule. In this case, we choose to describe each of the configuration classes using a FENE force law. Let us consider a molecule under flow (say, shear flow), that assumes a configuration (say, a folded state) with an end-to-end distance Q. In the presence of flow, the forces acting on any one of the beads are the

hydrodynamic drag force ($\mathbf{F}_i^H$), the elastic spring force ($\mathbf{F}_i^E$), and a random Brownian force ($\mathbf{F}_i^B$) imparted by the solvent molecules. The force balance on any bead in the chain is given by

$$\mathbf{F}_i^B + \mathbf{F}_i^E + \mathbf{F}_i^H = 0. \tag{3}$$

In the case of the end bead, $i=1$ or $i=N_b$. Averaging over several such chains (note that the average of the Brownian force will be equal to zero), we obtain

$$\langle \mathbf{F}_i^E \rangle + \langle \mathbf{F}_i^H \rangle = 0. \tag{4}$$

Here, we consider the forces acting on the N_b^{th} bead. The goal behind developing a dumbbell-like representation for this molecule is to describe the same configuration as a dumbbell connected by a FENE spring. Therefore, the elastic spring force can be replaced by the force exerted on the end bead due to the FENE spring, i.e., $\mathbf{F}_i^E = \mathbf{F}_i^{\text{FENE}}$. In the equivalent dumbbell (represented with the superscript d), the ensemble averaged force balance correspondingly on bead 2 can be written as

$$\langle \mathbf{F}_2^{H,d} \rangle + \langle \mathbf{F}_2^{\text{FENE}} \rangle = 0. \tag{5}$$

Subtracting Eqs. (3) and (5), we get

$$\langle \mathbf{F}_{N_b}^H \rangle = \langle \mathbf{F}_2^{H,d} \rangle + \langle \mathbf{F}_2^{\text{FENE}} \rangle - \langle \mathbf{F}_{N_b}^E \rangle. \tag{6}$$

The hydrodynamic drag force on the N_b^{th} bead can be written in terms of the coarse-grained parameter ζ_{conf}, while that of the dumbbell can be written in terms of the dumbbell bead drag coefficient (ζ_d) and is given by

$$\mathbf{F}^H = \zeta \dot{\gamma} (\boldsymbol{\kappa} \cdot \mathbf{R}_i), \tag{7}$$

where $\dot{\gamma}$ is the shear rate, $\boldsymbol{\kappa}$ is the dimensionless transpose of the velocity gradient tensor, and $\mathbf{R}_i$ is the position vector of the bead. The elastic force law can be written in a generic form as

$$\mathbf{F}^E = Hf(Q)\mathbf{Q}, \tag{8}$$

where H is the spring constant that varies based on the level of description (i.e., bead-spring or dumbbell model represented using subscript b-s or d, respectively); f is a scalar function that describes the nonlinear nature of the spring; and $\mathbf{Q}$ is the connector vector, with Q being its magnitude. Substituting Eqs. (7) and (8) into Eq. (6) we get

$$\frac{\zeta_{\text{conf}}}{\zeta_d} = 1 + \frac{1}{\zeta_d \dot{\gamma} |\langle \boldsymbol{\kappa} \cdot \mathbf{R} \rangle|} \left| \langle H_d f^{\text{FENE}}(R)\mathbf{R} \rangle - \langle H_{b\text{-}s} f(Q_{N_s})\mathbf{Q}_{N_s} \rangle \right|. \tag{9}$$

Since we are interested in sampling configurations present under flow, we study the configurations that the molecule assumes as it is exposed to standard flow conditions, namely, steady shear, and uniaxial extension. Figures 10 and 11 show the consolidated distribution of the lengths of molecules from various flow fields and configuration classes. The configurational distribution functions are very similar to one another for most configuration classes, except in the case of the stretched configuration class. The molecules under extensional flow attain a stretched state and are able to sample higher extensions due to the irrotational nature of the flow. Therefore, we observe a high probability for molecules in a highly stretched state. Further, there is a distribution of lengths for molecules in different configuration classes. Therefore, ideally, a configuration-based drag must also vary as a function of the length of the molecule in that configuration. However, initially, we investigate the applicability of a constant configurational drag by

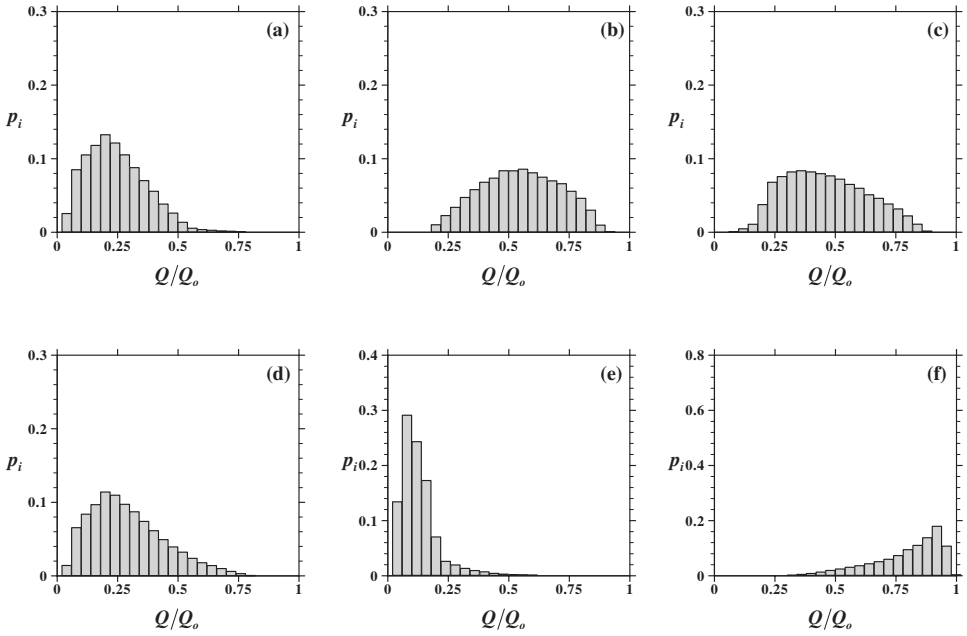

FIG. 10. Consolidated distribution of the end-to-end distance at different flow strengths for (a) folds, (b) half dumbbells, (c) kinks, (d) dumbbells, (e) coils, and (f) stretched configuration classes under steady shear.

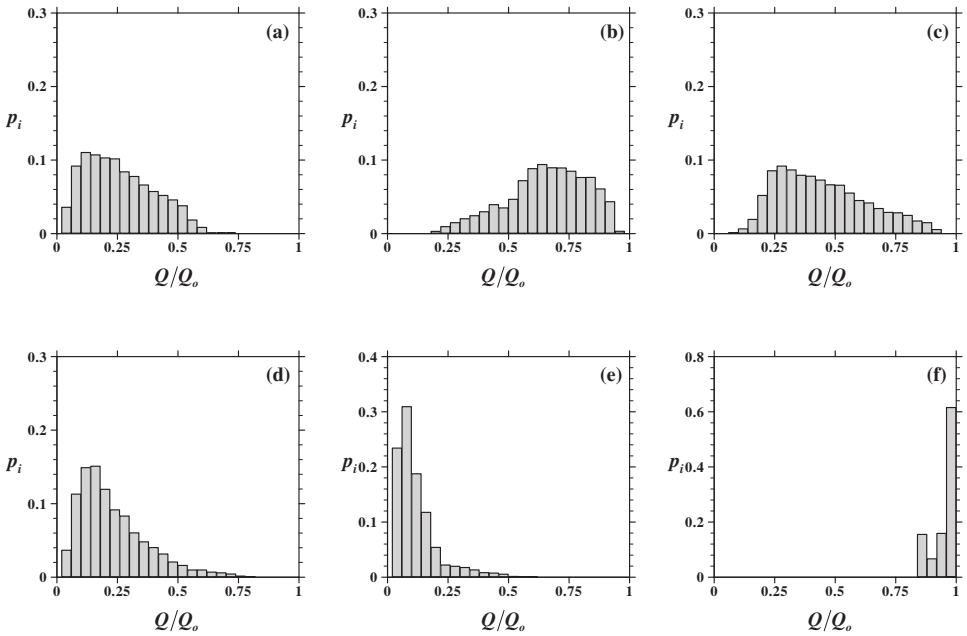

FIG. 11. Consolidated distribution of the end-to-end distance at different flow strengths for (a) folds, (b) half dumbbells, (c) kinks, (d) dumbbells, (e) coils, and (f) stretched configuration classes under steady uniaxial extension.

TABLE I. Drag coefficient for different configuration classes calculated using Eq. (9).

Configuration	$\zeta_{\text{conf}}/\zeta_d$
Fold	3
Half dumbbell	2
Kink	1.15
Dumbbell	4.3
Coil	1.4
Stretched	1.85

ensemble averaging over all possible end-to-end distances and overall flow strengths and flow types. For configuration classes wherein the distribution function is nearly Gaussian (half dumbbells and coils), such an assumption might be reasonable. However, for configuration classes where the distribution is skewed, a variable drag is required to accurately describe the variation as a function of length.

The drag coefficients calculated as described above, are presented in Table I. It is clear from our calculations that the drag coefficients of different configuration classes are indeed different. The values obtained for the drag coefficient can be explained by analyzing Eq. (9). We denote the first force term as term 1 and the second force term as term 2 and estimate their magnitudes. For the coiled configuration class, a single dumbbell model is sufficient to describe the dynamics of the molecule. Therefore, the magnitudes of terms 1 and 2 should almost be equal, yielding a drag coefficient close to 1. We find that the coiled configuration drag coefficient is slightly greater than 1. The larger drag coefficient is due to the sorting criteria used in the configuration sorting algorithm. In the automated algorithm, a limit is placed on the size of the molecule, i.e., all molecules smaller than a prescribed size are identified as coils. This limit may allow larger molecules which are truly not in coiled conformations, leading to a slightly greater value for the drag coefficient than the expected value. Moreover, since the ends of the coiled configuration have random orientations and the forces acting on the ends are also highly variable, the variance in term 2 is large, leading to uncertainties.

For kinked molecules, the springs at the ends of the chain are in a stretched state. In this case, the ensemble averaged force on the last bead, using either the FENE dumbbell model or the multibead-spring model, is very similar, yielding a drag coefficient close to unity. In order to understand the drag coefficient calculated for the folded, half dumbbell and stretched configuration, we also analyze the magnitude of the denominator. In all the three cases, term 2 is greater than term 1. However, the term in the denominator ($|\langle \boldsymbol{\kappa}\cdot\mathbf{R}\rangle|$) increases from the folded state to the half dumbbell state, and is the largest for the stretched state. The increase in the magnitude of the denominator is due to an increase in that of the end-to-end distance as we transition from a folded to a half dumbbell state to a stretched state. Correspondingly, we observe that the $\zeta_F/\zeta_d > \zeta_{\text{HD}}/\zeta_d > \zeta_S/\zeta_d$.

The drag coefficient for the dumbbell was found to be very large (close to two times that of the half dumbbell configuration). The observed large value can be reasoned based on the procedure used to calculate the drag coefficient. When a multibead-spring chain assumes a dumbbell configuration, the ends of the molecule are embedded in the coiled section of the molecule. Therefore, the magnitude of term 2 is relatively small. Moreover, since the ends of the molecule are close to equilibrium, the orientation of the end springs is almost random, leading to a large variance in the term $|\langle \boldsymbol{\kappa}\cdot\mathbf{R}\rangle|$, and in term 2. Alter-

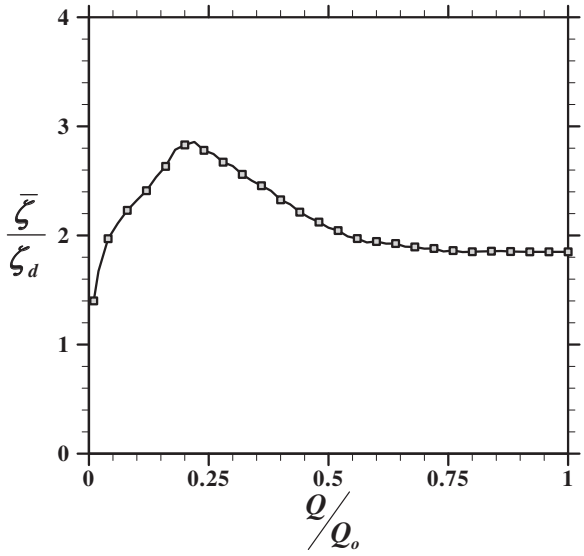

FIG. 12. Mean drag coefficient for the molecule as a function of the end-to-end distance calculated using the configuration-dependent drag calaculated from Eq. (9).

natively, the dumbbell configuration can be viewed as to be composed of two half dumbbells, leading to a drag coefficient which is near two times that of the half dumbbell. This is consistent with a drag coefficient of ≈ 4.

By using the average drag coefficients calculated for the different configuration classes, we estimate the variation of the mean drag coefficient of the molecule as a function of the end-to-end distance as

$$\frac{\bar{\zeta}}{\zeta_d}(Q) = \sum_{i=1}^{N_{\text{conf}}} p(i|Q)\frac{\zeta_i}{\zeta_d}. \tag{10}$$

Figure 12 reveals a nonmonotonic growth for the mean drag coefficient as we go from a coiled state to a stretched state. Larson *et al.* (1997) have calculated the increase in the drag on a molecule as it extends while an end of the molecule is tethered using optical tweezers and subjected to uniform flow. They found that the drag increases monotonically as the molecule unraveled from a coiled state to a stretched state. However, in the experiments, the flow was imposed so that the molecule unraveled in such a way that it aligned with the flow. In the method used above, the configurations of the molecule were obtained from different flow types and therefore included complex configurations. The observation of a nonmonotonic growth of the drag coefficient suggests a nonlinear configurational drag coefficient for dumbbells as a function of the end-to-end distance, especially in shearing flows.

2. Relaxation time

Modifying the relaxation time of the molecule is motivated by the fact that molecules of different lengths have differing relaxation times. Intuitively, it can be understood that the time taken by a fully stretched molecule to relax to a coiled state is different from that of a folded molecule. Since the relaxation time provides an estimate of the average time taken by a molecule to relax from its nonequilibrium state to its equilibrium state, it

directly suggests the concept of a configurational relaxation time. Therefore, developing a configuration-dependent relaxation time also provides a route to distinguish configuration classes from each other.

Conventionally, the relaxation time of a molecule is calculated by allowing an ensemble of fully stretched molecules to relax to their equilibrium configurations and fitting the tail of the relaxation of the tensile stress to a single exponential fit. This procedure has been successfully used by Doyle *et al.* (1997) to develop an empirical relationship for the relaxation time of a bead-rod chain as a function of the number of rods. It has also been used by Somasi *et al.* (2002) for calculating the relaxation time of bead-spring chains as a function of the degree of coarse graining. For the configuration based model, we are interested in calculating the relaxation time for the different configuration classes.

For instance, let us consider the folded configuration class. In this case, we start out with an ensemble of maximally stretched folded configurations and allow them to relax in the absence of flow. As the folded molecules relax, they change their configuration, populating other configuration classes. Consequently, calculating configuration dependent relaxation times is restricted by the fact that the molecules eventually become coiled. Although the existence of a configuration based relaxation time can be easily understood, its accurate determination is not feasible due to the problems posed by the phase space sampled by the molecule near equilibrium. Therefore, we do not consider the modification of the relaxation time as a possible route to identify configurational diversity. Instead, we choose to study its effect indirectly via the configuration-based drag coefficient.

3. Spring force law

The idea of a configuration-dependent spring force law can easily be understood by examining the following experiment. Let us consider a molecule that is constrained in a tube (i.e., it cannot make excursions outside the tube walls) that has a fixed configuration. The tube diameter is much larger than the Kuhn step size, thereby allowing the relaxation of the molecule at length scales smaller than the persistence length. The force required to fix the ends of the chain at the ends of the tube, while still allowing the intermediate sections of the molecule to move within, can be calculated as a function of the end-to-end distance of the tube (while retaining the gross configuration of the tube), yielding a force-extension law for that configuration class. It can directly be noted that based on the configuration of the tube that the molecule is constrained in, the force required to fix the ends of the molecule will vary, thereby suggesting a configuration-dependent spring force law. The idea is similar to that proposed initially using the constant extension ensemble, but it differs in that it specifically prescribes a overall configuration for the molecule. Although this provides a unique route to use the constant extension ensemble for configuration classes, it poses some complications due to the particular choice of the configuration of the tube. Therefore, we do not investigate this route for developing a coarse-grained model.

C. The model

The implementation of the configuration-based model using the configuration-dependent drag and the master configuration map is as follows. Initially, we start out with all dumbbells belonging to the coiled configuration. As the flow is imposed on the molecules, they extend and transition into different configuration classes. Correspondingly, the dumbbells are also extended and transition into different configurations classes. At any instant of time, the dumbbells are classified based on their end-to-end distances. The number of dumbbells with a given end-to-end distance that transition from the coiled

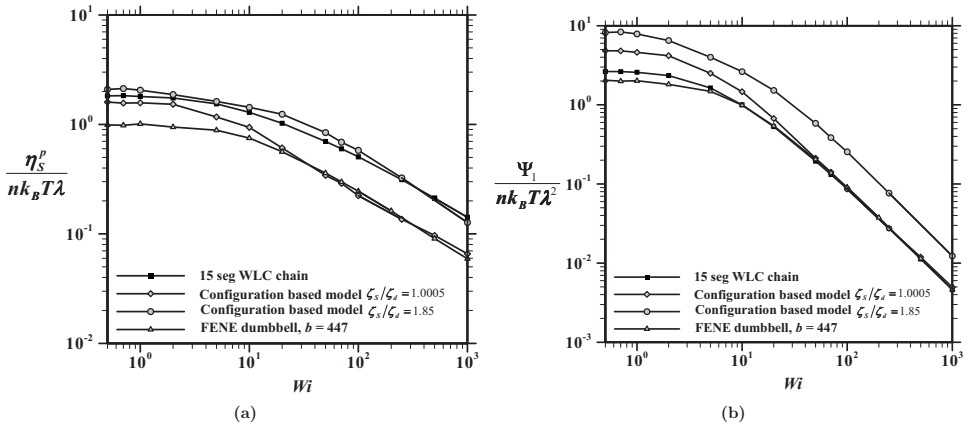

FIG. 13. (a) Polymer shear viscosity (η_S^p), scaled with ($nk_BT\lambda$), as a function of Wi for the configuration based model, FENE dumbbell model, and 15 segment WLC. (b) First normal stress coefficient (Ψ_1), scaled with ($nk_BT\lambda^2$), as a function of Wi for the configuration based model, FENE dumbbell model, and 15 segment WLC.

state to another state is calculated based on the previously generated MCM which prescribes the fraction of molecules that belong to a particular configuration class for a chosen end-to-end distance, $p(i|Q)$. The particular choice of molecules with a given end-to-end distance that will transition from configuration class A at time instant t to configuration class B at time instant $t+\delta t$, is arbitrarily decided upon as long as the partitioning of the molecules is in agreement with the conditional probabilities calculated *a priori*. Once the dumbbells have been assigned their new configuration classes, they are described using the corresponding configurational drag and therefore evolve differently from one another. The procedure is repeated until the distribution of configurations reaches a steady state, which directly indicates the attainment of steady state for the flow itself. The probability of occurrence of a configuration class at any instant of time can again easily be calculated by adding the total number of dumbbells over all end-to-end lengths that belong to a particular configuration class and dividing it by the total number of trajectories that were simulated. Moreover, the distribution of the end-to-end distances for each configuration class or for the entire ensemble of molecules can easily be calculated by binning the simulated trajectories.

IV. RESULTS

In this section, we present predictions for the configuration-based model (CBM) using the configuration-dependent drag, in conjunction with the configuration map. We compare the results with the underlying 15 segment bead-spring chain, and with the FENE dumbbell model, to elucidate the advantages of the configuration-based model over the simplistic FENE dumbbell model. The models are matched by maintaining the same contour length for the molecule. We study the start-up of steady shear, and uniaxial extensional flow.

A. Steady shear flow

In steady shear, the velocity field is given as, $v_x = \dot{\gamma} y$, $v_y = v_z = 0$, where, $\dot{\gamma}$ is the shear rate. The shear viscosity and first normal stress coefficient for the configuration based model, FENE dumbbell model and the underlying 15-segment worm-like chain (WLC) are presented in Figs. 13(a) and 13(b), respectively. The shear viscosity predicted by the

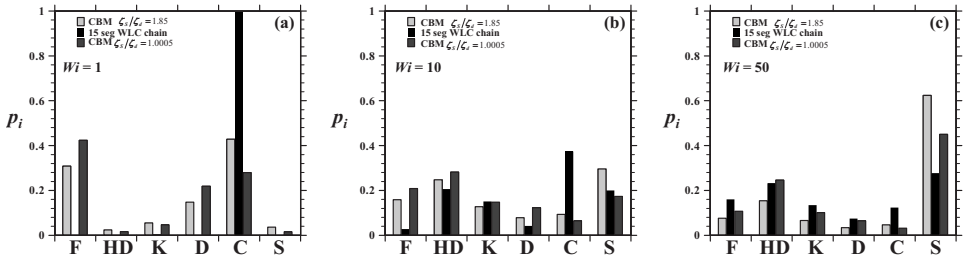

FIG. 14. Configurational probability distribution in steady shear for the configuration based model and the 15 segment WLC for (a) Wi=1, (b) Wi=10, and (c) Wi=50.

configuration based model is in good agreement with the underlying multisegment chain. The critical shear rate, corresponding to the onset of shear thinning, is at higher Wi for the configuration based model. However, the first normal stress coefficient is overpredicted by the configuration based model over the entire range of shear rates studied. On the other hand, the shear viscosity of the FENE dumbbell model is underpredicted for all Wi, while the first normal stress coefficient is in good agreement with the multibead-spring model, except at very low Wi.

In order to understand the effect of using a configuration-based drag coefficient, we arbitrarily modify the drag coefficient for the stretched state (i.e., $\zeta_S/\zeta_d=1$). The predictions using this modified drag coefficient, while retaining the drag coefficients for other configuration classes from our earlier calculations, are also presented in Figs. 13(a) and 13(b). We observe that the zero-shear viscosity is in close agreement with the multibead-spring model, while the shear viscosity in the shear-thinning regime decreases to that of a FENE dumbbell model. Similarly, the first normal stress coefficient is over predicted at low Wi, but is in agreement with the multibead-spring model at large Wi. The contribution of a particular configuration class to the total viscosity can be directly understood using this method. At low Wi, the probability of occurrence of a stretched state is negligible. Therefore, the modification of the stretched state drag coefficient does not affect the observed macroscopic properties. However, at higher Wi, the molecule samples the stretched state as it tumbles. Therefore, the modification of the drag coefficient, to approach the FENE dumbbell drag coefficient, directly leads to a response that is close to the FENE dumbbell predictions.

The predictions from the configuration based model are insightful in understanding the deficiencies of a simplistic dumbbell model, such as the FENE model. It is clear from our simulations, that configurational diversity is the crucial element for obtaining accurate predictions for the shear viscosity. The shear viscosity is indirectly related to the thickness of the molecule in the direction transverse to the flow that it occupies as it tumbles under shear flow. The dumbbell model is inherently deficient due to the lack of internal degrees of freedom. The lack of internal modes leads to an inaccurate prediction for the transverse direction thickness, thereby leading to an underprediction of the shear viscosity. On the other hand, the configuration based model, incorporates multiple relaxation modes by modifying the drag properties of the dumbbells belonging to the different configuration classes. We observe that the mean of the transverse direction thickness is comparable for the multisegment model and the configuration based model. However, the stretch along the direction of flow for the configuration based model is greater than the stretch for the bead-spring chain. This explains the overprediction of the first normal stress coefficient.

Figure 14 shows the configurational probability distributions for the bead-spring chain

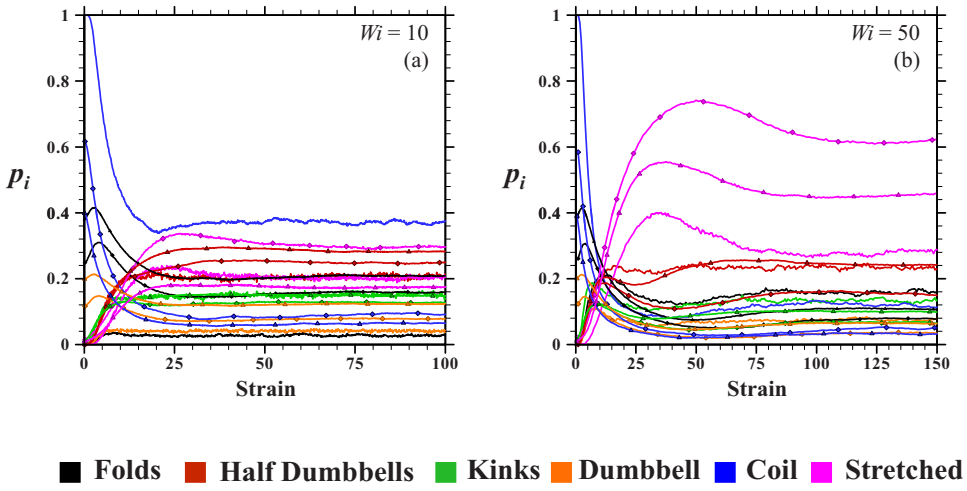

FIG. 15. Evolution of configurational probabilities as a function of strain in steady shear flow for the configuration based model (i) ζ_S/ζ_d=1.85, ◇ (ii) ζ_S/ζ_d=1, △), and the 15 segment WLC (solid lines) at (a) Wi=10 and (b) Wi=50.

and the configuration based model at Wi=1, 10, and 50. At lower Wi, folded and dumbbell states are predicted by the configuration based model, which are not observed for the bead-spring chain. These configuration classes are spurious and arise due to the configuration map developed earlier. It can be noted that the configuration map (Fig. 9) also shows a finite probability for folded states at very low extensions. This probability is not inaccurate, as such, since folded states can exist at low extensions, especially in shear flow (as the molecule tumbles). However, these states are not accessible to the molecule at equilibrium. The nature of the configuration map does not differentiate between these two cases, and that is the reason for the observed configurational probabilities even at low Wi. However, the inclusion of these configuration classes at low Wi provides an accurate prediction for the shear viscosity, suggesting that the drag coefficient of molecules at low Wi is indeed different from that of a FENE dumbbell. At Wi=10, the configuration based model provides reasonable predictions for most configuration classes, except the folded and coiled configurations. This has been reasoned earlier to arise from the nature of the configuration map. At high Wi, the configurational based model predicts configurational probabilities in good agreement with the multibead-spring model, except for the stretched state. The overprediction of the first normal stress coefficient can be viewed to arise from this.

We present the evolution of the configurational probabilities as a function of strain for Wi=10 and Wi=50 in Fig. 15. The initial dynamics for half dumbbell, kinked, and stretched configurations are captured well by the configuration based model. However, at steady state, the configurational probability for the stretched state is overpredicted. The initial dynamics for the other two configuration classes are inaccurate due to deficiencies in the configuration map that have been stated earlier. The growth of the shear stress and tensile stress for Wi=10 and Wi=50 are presented in Fig. 16. The steady state shear stress is in close agreement with that of the multibead-spring model. The overshoot for the shear stress is overpredicted by the configuration based model, especially at higher Wi. This may be due to the faster unraveling of molecules using the configuration based model. On the other hand, the FENE dumbbell model underpredicts the shear stress as well as the overshoot. The tensile stress is severely overpredicted by the configuration

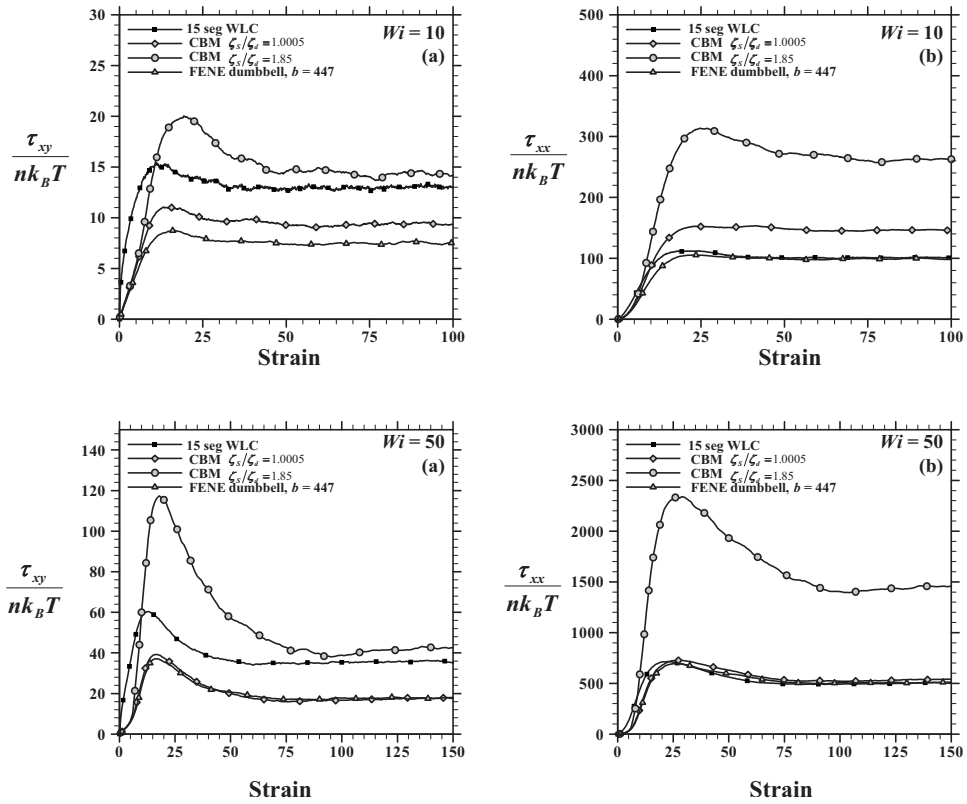

FIG. 16. Evolution of (a) shear stress (τ_{xy}) and (b) tensile stress (τ_{xx}), scaled with (nk_BT), with strain in steady shear at Wi=10 and Wi=50.

based model in comparison to the multibead-spring model, while the FENE dumbbell provides reasonable comparisons for the tensile stress. The configuration-based model with the modified drag coefficient ($\zeta_S/\zeta_d=1$) clearly identifies the source for the overprediction of normal stresses and the overshoots in the shear and tensile stress. Using the modified drag coefficient, the configuration-based model is very close in predictions to the FENE dumbbell model.

Two conclusions can be inferred from our simulations using the configuration based models, i.e., for $\zeta_S/\zeta_d=1.85$ and $\zeta_S/\zeta_d=1$. The configuration dependent drag coefficient is necessary to obtain an accurate prediction of the shear viscosity. However, this leads to an overprediction of the tensile stress. On the other hand, the configuration based model with $\zeta_S/\zeta_d=1$ provides a good prediction for the tensile stress. It is known that the shear stress is related to the transverse direction thickness of the molecule, while the tensile stress is related to the stretch of the molecule along the flow direction. In order to obtain agreement between the CBM and the fine-grained bead-spring model for both the shear and tensile stress, it can therefore be deduced that, the drag along the flow and transverse directions should be different. The use of an anisotropic drag should be successful in correcting the deficiencies of the configuration based model. It will be explored in a subsequent publication.

B. Start-up of uniaxial extensional flow

The velocity field in uniaxial extensional flow is given as $v_x=\dot{\epsilon}x$, $v_y=-(\dot{\epsilon}/2)y$, and $v_z=-(\dot{\epsilon}/2)z$, where $\dot{\epsilon}$ is the extension rate. We present the extensional viscosity for the

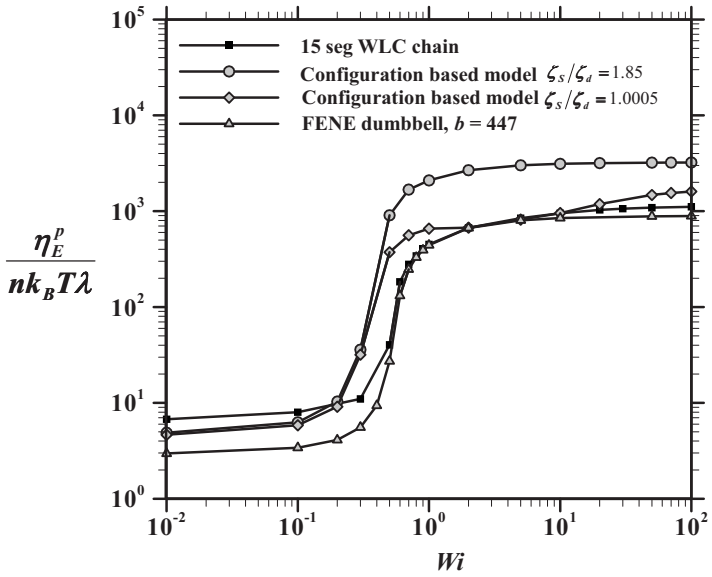

FIG. 17. Polymer extensional viscosity (η_E^p), scaled by ($nk_BT\lambda$), as a function of Wi.

configurational based model ($\zeta_S/\zeta_d = 1.85$ and $\zeta_S/\zeta_d = 1$) in Fig. 17. At low Wi, the extensional viscosity is three times the shear viscosity. The configuration based model predicts a slightly lower plateau at low Wi, in comparison to the bead-spring model. However, it is still an improvement over the FENE dumbbell model. Past the coil-to-stretch transition, the configuration-based model overpredicts the extensional viscosity for all extension rates studied here. However, the FENE dumbbell model is in close agreement with the multibead-spring model beyond the coil-to-stretch point. The configuration based model with the modified drag coefficient ($\zeta_S/\zeta_d = 1$) shows good agreement with the multibead-spring model at high Wi.

The overprediction of the viscosity can be related to the stretch of the molecule along the direction of extension. Figure 18 shows the evolution of the tensile stress and *xx* component of the conformation tensor. At both the Wi shown here, the configuration based model overpredicts the tensile stress. At Wi = 1, the FENE dumbbell model also overpredicts the stress, while it closely follows the multibead-spring model at Wi = 10. The *xx* component of the conformation tensor is overpredicted by all the models at Wi = 1 and Wi = 10.

The differences in the tensile stress and conformation of the molecule are more pronounced when studying stress-conformation hysteresis. It is known that the relaxation of stress and configuration occur at different rates leading to a hysteresis in the behavior of molecules as they relax after stretching during uniaxial extension. The stress-conformation hysteresis for all models are presented in Fig. 19 at Wi = 1 and Wi = 10. The configuration-based model shows a very large stress-conformation hysteresis due to the overprediction of both the stresses and conformation. However, the modification of the drag property for the stretched state reduces the size of the stress-conformation hysteresis curve. Past the coil-to-stretch transition, in uniaxial extension flow, the molecules exist in the stretched configuration only. Therefore, the modification of the drag coefficient corresponding to the stretched state immediately reduces the predictions of the configuration-based model to closely follow the FENE dumbbell model. The existence of

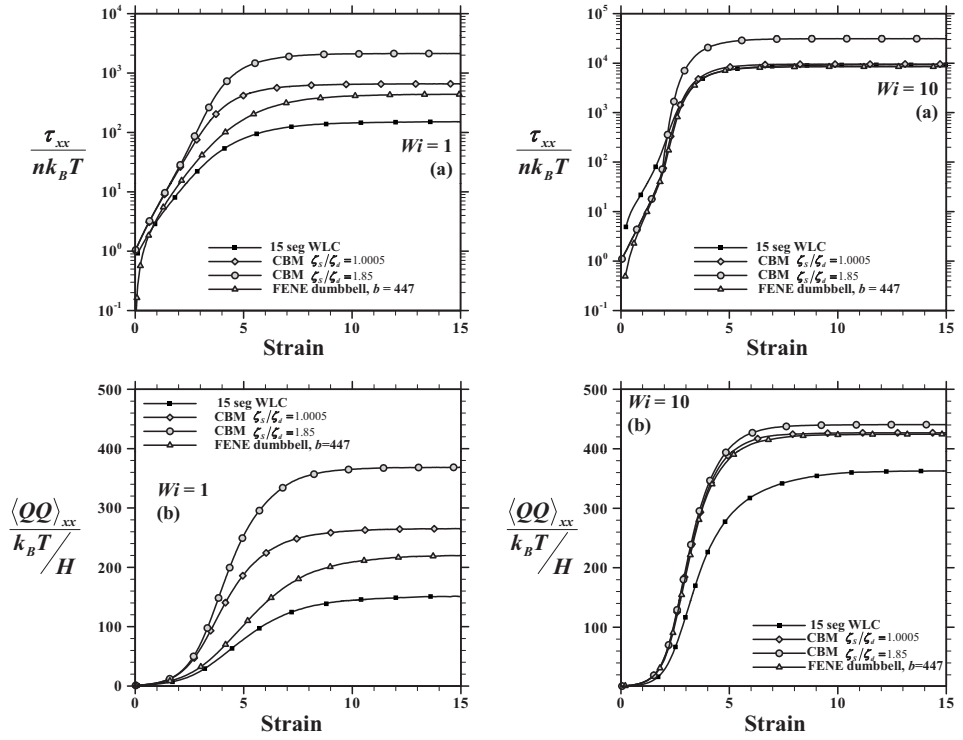

FIG. 18. Evolution of the (a) tensile stress (τ_{xx}), scaled with (nk_BT), and (b) xx component of the conformation tensor ($\langle \mathbf{QQ} \rangle_{xx}$), scaled with k_BT/H, as a function of strain for Wi=1 and Wi=10.

internal modes in the bead-spring model leads to a large stress for smaller extensions. Again, the idea of an anisotropic drag should be useful in obtaining closer prediction for the conformation of the molecule, while retaining the drag coefficient of the FENE dumbbell for the stretched state along the flow direction.

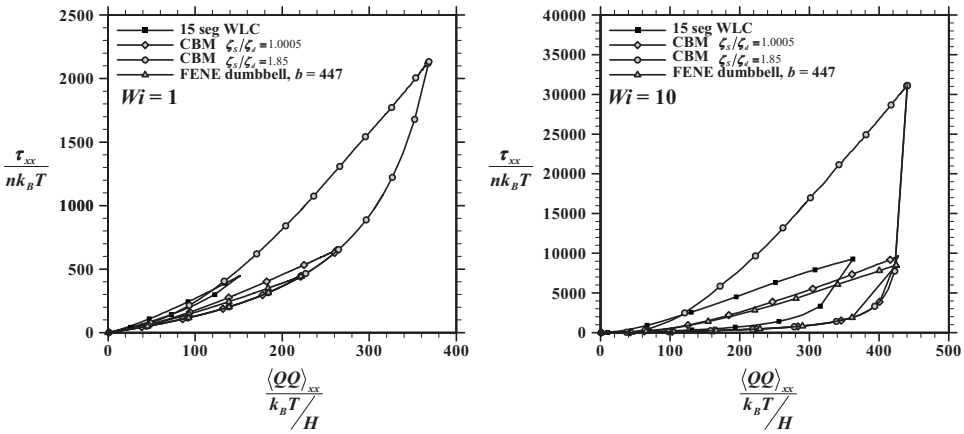

FIG. 19. Stress-conformation hysteresis for the configuration based model, FENE dumbbell model, and 15 segment WLC at Wi=1 and Wi=10.

V. SUMMARY

A configuration-based, coarse-grained model was developed for studying the dynamics of macromolecular solutions. The importance of the inclusion of configurational information into a simplistic dumbbell model was explored by studying the configurations of the molecules under steady shear and uniaxial extension and relating configurational distributions to observed macroscopic properties. The configuration-based model was thus developed based on the existence of a few predominant configuration classes that are present in all flow types. These classes were used to partition the configurational phase space of the molecule. The macromolecules were described using a single dumbbell description with varying drag coefficients based on the configuration they represented. The probability distribution of configurations under any flow type was derived based on a configuration map. The configuration map was derived by exploring the configuration phase space sampled by the molecule under different flow types and strengths. It was found that the conditional probability for finding a molecule in a given configuration class for a fixed end-to-end distance was universal. Therefore, the partitioning of molecules into the different configurations must always be in accordance with the configuration map.

The predictions for the configuration-based model were studied using the BD approach under steady shear and uniaxial extension. The model provides good predictions in comparison to the underlying multibead-spring model for the shear viscosity while overpredicting the first normal stress coefficient. Modifying the stretched state drag coefficient provided an insight into the reason behind the overpredictions. The overprediction in the tensile stress was found to be due to the overprediction of the xx component of the conformation tensor. On the other hand, a good prediction for the shear stress in comparison to the FENE dumbbell model indicated that the modified drag coefficients were crucial to obtain agreeable predictions for the shear stress. Similarly, in uniaxial extension, the tensile stress as well as the xx component of the conformation tensor were overpredicted. This again was tied to the drag coefficient of the stretched state which led to an excessive prediction for the stretch of the molecule. A reduced drag coefficient for the stretched state yielded improvements in the prediction of macroscopic as well as microscopic properties along the direction of flow while the calculated drag coefficients provided a good prediction for the shear stresses. These findings emphasize the fact that configuration classes must not merely be treated as differently sized objects but as differently shaped objects as well. Therefore, the use of an anisotropic drag which accounts for the difference in average dimension of the configuration along and traverse to the direction of flow could achieve good comparisons for both the shear stress and tensile stress with a fine-scale model and forms part of the future work to improve the model. Another aspect that could possibly lead to a fine-tuned model is the development of guidelines for the use of the configuration map that would prevent the sampling of configurations other than the coiled state upon inception of flow from equilibrium.

The configuration-based, coarse-grained model presents a novel way to incorporate configurational diversity into a simplistic dumbbell model. It holds promise for studying macromolecular dynamics in complex flow studies which has historically been limited to dumbbell-based models due to computational limitations. The model molecule studied here is representative of the procedures for the development of model tools required for the implementation of the model. The use of the model for studying the flow of any macromolecule in a complex flow geometry would therefore involve two steps. The first step involves the development of the configuration map corresponding to the macromolecule of choice and the calculation of modified drag coefficients for the configuration

classes for that macromolecule. The second step is to use the tools developed in the first step to implement the configuration-based model in the complex flow calculation just like any other dumbbell model. Although the first step may seem cumbersome, as it has been pointed out earlier, investigating the dynamics in steady shear, uniaxial, and biaxial extension is sufficient to obtain a relatively accurate configuration map and configuration dependent drags. With the model parameters and configuration map developed, the use of the model for studying macromolecular flows in complex geometries can be realized.

APPENDIX

1. Governing equations

In the BD approach, the solvent is described as a continuum with a prescribed viscosity that randomly collides with the macromolecule, the effect of which is modeled as a stochastic force imparted on the macromolecule. On the other hand, the macromolecule is explicitly modeled either as a bead-rod chain, bead-spring chain, or a dumbbell [Bird *et al.* (1987a)]. The governing equation for the evolution of the extension of the macromolecule is obtained by writing a force-balance on each bead and solving for the position of the beads simultaneously. Macroscopic observables are then computed as a function of the bead positions.

In the case of the bead-rod model, the macromolecule is represented as N_k+1 identical beads connected by rods of length a while in the bead-spring model, the macromolecule is represented as N_b identical beads connected by N_s springs. The position vector representing the position of bead i with respect to an arbitrary point fixed in space is represented as $\mathbf{r}_i$. Neglecting inertia for time scales larger than the momentum relaxation time, the governing equation for the motion of the beads is obtained by writing a force balance on the bead i as given in Eq. (3) where the elastic spring force can be replaced by the connector vector force ($\mathbf{F}_i^C$) which is due to the tension in the rods in the case of the bead-rod model and due to the elastic force exerted by the springs in the case of the bead-spring model.

In the absence of hydrodynamic interactions, the hydrodynamic drag force on bead i is given by

$$\mathbf{F}_i^H = -\zeta(\dot{\mathbf{r}}_i - \mathbf{u}_i^\infty), \tag{A1}$$

where ζ is the bead drag coefficient, $\dot{\mathbf{r}}_i$ is the velocity of bead i, and $\mathbf{u}_i^\infty$ is the solvent velocity at bead i.

In the bead-spring model, the connector vector force ($\mathbf{F}_i^C = \mathbf{F}_i^S$) is due the springs that are attached to the beads and the effective spring force on bead i is given by

$$\begin{aligned} &= \mathbf{F}_1^{Sp} \quad i = 1, \\ \mathbf{F}_i^S = \mathbf{F}_i^{Sp} - \mathbf{F}_{i-1}^{Sp} \quad &i = 2, \ldots, N_b - 1, \\ &= -\mathbf{F}_{N_s}^{Sp} \quad i = N_b, \end{aligned} \tag{A2}$$

while in the case of a bead-rod model, the connector vector force ($\mathbf{F}_i^C = \mathbf{F}_i^T$) is due to the tension in the rods connected to the bead. This is given by

$$\mathbf{F}_i^T = T_i \mathbf{u}_i - T_{i-1}\mathbf{u}_{i-1}, \tag{A3}$$

where T_i is the tension in rod i and $\mathbf{u}_i$ is the orientation vector between beads i and $i+1$. The Brownian force is mathematically represented as a quantity with a zero mean

and a second moment that balances the dissipative forces to satisfy the fluctuation dissipation theorem

$$\langle \mathbf{F}_i^B \rangle = 0, \tag{A4}$$

$$\langle \mathbf{F}_i^B(t)\mathbf{F}_j^B(t+\delta t)\rangle = 2k_BT\zeta\delta_{ij}\delta(\Delta t) \approx \frac{2k_BT\zeta\delta_{ij}}{\Delta t}, \tag{A5}$$

where k_B and T are the Boltzmann constant and temperature.

Combining the above description of forces acting on a bead in Eq. (A5), the equation governing the motion of bead i can be written as

$$0 = \zeta(\mathbf{u}_i^\infty - \dot{\mathbf{r}}_i) + \sqrt{\frac{2k_BT\zeta}{\Delta t}}d\mathbf{W}_i' + \mathbf{F}_i^{S/T} + \mathbf{F}_i^{\text{Ext}}, \tag{A6}$$

where $d\mathbf{W}_i'$ is a Wiener process mathematically represented by a Gaussian random number with a zero mean and unit variance. Equation (A6) can be rearranged to give the time evolution of the position vectors ($\mathbf{r}_i$) of the beads

$$d\mathbf{r}_i = \sqrt{\frac{2k_BT}{\zeta}}d\mathbf{W}_i + \left[\mathbf{u}_i^\infty + \frac{\mathbf{F}_i^{S/T}}{\zeta} + \frac{\mathbf{F}_i^{\text{Ext}}}{\zeta}\right]dt, \tag{A7}$$

where $d\mathbf{W}_i$ is a Gaussian random number with a zero mean and variance of Δt.

The stochastic differential Eq. (A7) for the bead-rod model has to be solved along with the imposition of constraints on the rods to maintain the distance between any two beads at the length of the rods

$$(\mathbf{r}_{i+1} - \mathbf{r}_i)\cdot(\mathbf{r}_{i+1} - \mathbf{r}_i) - a^2 = \phi^2, \tag{A8}$$

where ϕ^2 is a specified tolerance criterion ($\sim 10^{-6}$–10^{-8}). The governing equation is nondimensionalized using the following scales. The length scale used is the length of a rod (a), the time scale used is the bead diffusion time ($\zeta_{b-r}a^2/k_BT$), and the forces are nondimensionalized using k_BT/a. The resulting evolution equation is

$$d\mathbf{r}_i^* = [\text{Pe}(\boldsymbol{\kappa}\cdot\mathbf{r}_i^*) + F_i^{T,*} + \mathbf{F}_i^{\text{Ext},*}]dt^* + \sqrt{2}d\mathbf{W}_i, \tag{A9}$$

where $\boldsymbol{\kappa}$ is the transpose of the dimensionless velocity gradient tensor. The specific form of $\boldsymbol{\kappa}$ for simple shear and uniaxial extensional flow are given below

$$\boldsymbol{\kappa}_{\text{shear}} = \begin{bmatrix} 0 & 1 & 0 \\ 0 & 0 & 0 \\ 0 & 0 & 0 \end{bmatrix}; \quad \boldsymbol{\kappa}_{\text{ext}} = \begin{bmatrix} 1 & 0 & 0 \\ 0 & -\frac{1}{2} & 0 \\ 0 & 0 & -\frac{1}{2} \end{bmatrix}. \tag{A10}$$

The starred quantities represent dimensionless variables. Nondimensionalization of the governing equation leads to a dimensionless quantity—the Peclet number [Pe $=(\dot{\gamma}\zeta a^2/k_BT)$], which is the dimensionless shear/extension rate and is calculated as the ratio of the Weissenberg number (Pe=Wi/λ*) and the dimensionless relaxation time of the molecule. The relaxation time of the molecule has been previously calculated via simulation and fit to an expression by Doyle *et al.* (1997) and is used here. The solution procedure for the above equations is adopted from Somasi *et al.* (2002).

The polymer contribution to the stress can be calculated once the positions of the beads have been calculated using the Karmers–Kirkwood expression as

$$\boldsymbol{\tau}_p = n_p \sum_{i=1}^{N_k+1} \langle \mathbf{R}_i \mathbf{F}_i^H \rangle, \tag{A11}$$

where n_p is the number density of polymer chains and $\mathbf{R}_i$ is the position vector of the bead i relative to the center of mass of the chain

$$\mathbf{R}_i = \mathbf{r}_i - \mathbf{r}_c, \tag{A12}$$

where

$$\mathbf{r}_c = \frac{1}{N_k+1} \sum_{i=1}^{N_k+1} \mathbf{r}_i. \tag{A13}$$

In the case of the bead-spring model, it is easier to study the evolution of the connector vectors since the position of the chain in space is arbitrary and it is the relative positions of the beads with respect to each other that are of importance. The evolution equation for the connector vector ($\mathbf{Q}_i$) can be derived by subtracting the equations for the evolution of $\mathbf{r}_{i+1}$ and $\mathbf{r}_i$ and is given by

$$d\mathbf{Q}_i = \left[\mathbf{u}_i^{\infty} + \left(\frac{\mathbf{F}_{i+1}^S - \mathbf{F}_i^S}{\zeta} \right) + \left(\frac{\mathbf{F}_{i+1}^{\mathrm{Ext}} - \mathbf{F}_i^{\mathrm{Ext}}}{\zeta} \right) \right] dt + \sqrt{\frac{2k_BT}{\zeta}} (d\mathbf{W}'_{i+1} - d\mathbf{W}'_i). \tag{A14}$$

The length scale used is the equilibrium length of a Hookean spring ($\sqrt{k_BT/H}$), the time scale used is the relaxation time of the Hookean spring ($\zeta/4H$) and the forces are nondimensionalized using $\sqrt{k_BTH}$. The dimensionless SDE thus obtained is

$$d\mathbf{Q}_i^* = \left[\mathrm{Pe}(\boldsymbol{\kappa} \cdot \mathbf{Q}_i^*) + \left(\frac{\mathbf{F}_{i+1}^{S,*} - \mathbf{F}_i^{S,*}}{4} \right) + \left(\frac{\mathbf{F}_{i+1}^{\mathrm{Ext},*} - \mathbf{F}_i^{\mathrm{Ext},*}}{4} \right) \right] dt + \sqrt{\frac{1}{2}} (d\mathbf{W}_{i+1} - d\mathbf{W}_i), \tag{A15}$$

where $\mathrm{Pe} = \dot{\gamma}\zeta/4H$. The Peclet number is a measure of the dimensionless flow strength and is calculated as the ratio of the Weissenberg number to the dimensionless relaxation time ($\mathrm{Pe} = \mathrm{Wi}/\lambda^*$). Here, the dimensionless longest (λ^*) relaxation time is calculated by fitting the tail of the relaxation of tensile stress to a single exponential fit of the form

$$\tau_{xx}^* = A \exp\left(-\frac{t^*}{\lambda^*} \right) + B. \tag{A16}$$

In order to study the diversity of the configurational phase space, BDS is carried out by starting initially with many trajectories (typically 10^4–10^5) described using the bead-spring or bead-rod model. The initial configuration of each trajectory is randomly assigned, thereby selecting independent evolution paths for each molecule. Initially, the trajectories are allowed to attain the equilibrium distribution by allowing the ensemble to evolve in the absence of flow for a couple of relaxation times of the molecule. The equilibrium ensemble is then exposed to flow, and the evolution of the trajectories is monitored. At any instant of time, macroscopic properties can be evaluated by appropriate ensemble averaging, and configurational distributions are obtained using the automated configuration sorting algorithm described in the following section.

2. Model parameters

The λ-DNA molecule has a length of 21.2 μm [Smith *et al.* (1999)] and is represented using a 15-spring chain, coarse grained from a 150 bead-rod ($N_k = 150$) chain. The num-

ber of rods used to describe the molecule is calculated based on the Kuhn step size (b_K). The Kuhn step length is around 0.132 μm [Hur *et al.* (2000)], yielding around 150 Kuhn segments. The force-extension behavior of the molecule follows the Marko–Siggia expression [Marko and Siggia (1995)], also known as the WLC force law. It is given as

$$\mathbf{F}_i^s = \frac{k_B T}{b_K}\left[\frac{1}{2}\frac{1}{\left(1-\frac{Q_i}{Q_o}\right)^2} - \frac{1}{2} + \frac{2Q_i}{Q_o}\right]\frac{\mathbf{Q}_i}{Q_i}, \tag{A17}$$

where $\mathbf{Q}_i$ is the connector vector between two beads, Q_i is its magnitude, Q_o is the maximum length of the spring, k_B is the Boltzmann constant, and T is the temperature. The maximum extensibility is the square of the maximum length of the molecule [$b = Q_o^2/(k_B T/H_s)$] and is calculated by

$$b = 3(N_k - 1) \tag{A18}$$

to be 447 [Hur *et al.* (2000)]. The maximum extensibility for the individual springs b_s is given by $b_s = b/N_s = 29.8$. The longest relaxation time of the chain in dimensionless terms is [Somasi *et al.* (2002)]

$$\lambda_d = \frac{\lambda}{(\zeta/4H_s)} = 34.996, \tag{A19}$$

where ζ is the bead drag coefficient and H_s is the Hookean spring constant.

3. Automated configuration sorting algorithm

In this section, we present the automated configuration sorting algorithm used to identify configurations from a BDS of a multibead-spring chain. The configuration of a molecule is assigned based on a brightness distribution which is calculated based on bond and bead overlaps. The calculation of a brightness distribution is motivated from the experimental observation of molecular configurations. Under the microscope, coiled molecules appear as bright, compact blobs; while stretched molecules appear lighter and linear. The model molecule, at any instant of time, is described as a set of N_b beads connected by N_s springs or N_k rods of known orientations. The relative positions of the beads along the backbone of the molecule can be calculated by placing the origin at the center-of-mass of the molecule.

The first step in calculating the brightness distribution is to calculate the brightness due to bond overlap. For this purpose, the direction of maximum extension along the chain is calculated and is chosen as the axis along which the brightness distribution will be evaluated. In the case of uniaxial extension, this step is not very important since the molecule extends only along the direction of the flow. Calculating a brightness distribution along the direction of the flow does provide a good prediction for the configuration of the molecule. However, in shearing flows, the molecule tends to tumble and move along the shear-gradient direction. Calculating a brightness distribution based on the direction of shear would not provide a good prediction for the configuration since excursions along the shear-gradient plane will be projected into the direction of shear, giving rise to incorrect predictions for the configuration. The springs are therefore projected along the direction of maximum extension of the molecule in order to calculate the brightness distribution. Once the axis of the brightness distribution is calculated, a value of one is added along the brightness axis if a spring is present. Therefore, in cases where the molecule turns around or bends, there will be a bond overlap leading to a brightness value of 2 in those regions.

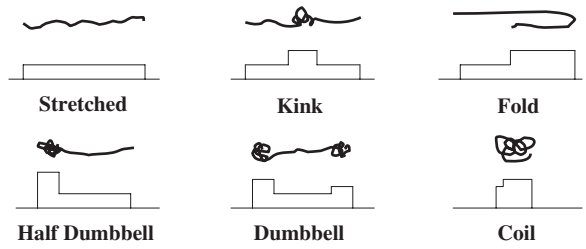

FIG. 20. Schematic of configuration classes considered along with representative brightness distribution plots.

The first step provides an estimate for the changes along the contour of the molecule. The bead-spring description of the molecule also involves springs which are elastic, to account for the loss of degrees of freedom when coarse graining from a bead-rod description. A compressed spring would indicate configurational kinks in the underlying bead rods, while a stretched spring would imply a straight set of rods. Therefore, accounting for bead overlap which occurs due to the existence of compressed springs is necessary in the bead-spring model to account for the configurational diversity existent at finer scales that cannot be discerned due to coarse graining in the bead-spring model. In the case of a bead-rod model, such as the Kramers model, this step would not be required since the rods are of constant length. In order to account for bead overlap, we need an estimate for the bead radius. The bead radius is calculated based on the fact that at equilibrium, the beads cannot overlap. Since the distance between two bead centers is given by the extension of the spring, the bead radius is assigned as the equilibrium length of a Hookean spring. When two beads overlap, the brightness is increased by a unit value in the corresponding region.

For the purpose of implementing the above algorithm, the brightness axis is initially divided into a large number of bins. The length scale of the bins is much smaller than the equilibrium length of a Hookean spring. The brightness value for each bin is determined based on the bead/bond overlap occurring in that region on the scale of the bin size. Once the brightness distribution is calculated as described above, it is smoothed (by taking a mean over a couple of bins) in order to obtain a coarse-scale brightness distribution that can be used for automated assignment of configuration classes. The criteria used for automated assignment of configurations are adopted from earlier work by Larson *et al.* (1999). The configuration classes considered in this work are inspired by observations in experiments that have indicated the existence of similar configuration classes [Smith and Chu (1998); Schroeder *et al.* (2003)]. A schematic of the configuration classes and representative brightness distribution plots are presented in Fig. 20.

Looking at the ends of the chain, if the brightness is unity at one end and greater than unity at the other end, the molecule can be a fold (F) or a half dumbbell (HD). If $y/x > 1/4$, the molecule is assigned a folded state, while if $y/x < 1/4$, the molecule is considered as a half dumbbell (y is the length of the brightness distribution with brightness greater than unity, x is the total length of the brightness distribution). If the brightness at both ends of molecule is unity, the molecule is either stretched (S) or kinked (K). In this case, we look at the brightness of the molecule in the middle of the brightness distribution. If it is unity throughout, it is considered as stretched, otherwise, as kinked. Finally, if the brightness at both ends of the distribution is greater than 1, the molecule is either a coil (C) or a dumbbell (D). In this case, we study the brightness distribution in the middle of the molecule, and if it is of unit value in the middle, the molecule is assigned a dumbbell state, otherwise, as a coiled state.

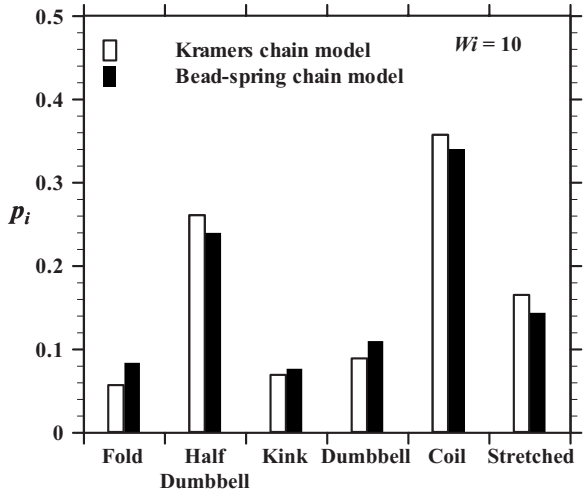

FIG. 21. Comparison of the probability of occurrence of different configuration classes at steady state under steady shear flow at Wi = 10 for a bead-spring model with a bead-rod model for the λ-phage DNA molecule.

In order to evaluate the accuracy of the configuration sorting algorithm, we compare the prediction for the probability of occurrence of a configuration class in steady shear flow at Wi = 10 using a bead-spring model with the prediction for the bead-rod model. As pointed out earlier, while using the above algorithm to ascertain the configuration of a molecule described using a bead-rod model, we do not consider bead overlap since the rods are of fixed length. However, when comparing the configurational distributions from a bead-spring model with those from a bead-rod model, it is important that we compare them at the same level of coarse graining. Therefore, for the case of the Kramers model, an equivalent bead-spring chain is constructed using the coarse-graining criteria presented by Somasi *et al.* (2002), i.e., we only consider every tenth bead and ignore intermediate beads. Using the equivalent bead-spring chain for the underlying bead-rod chain, we evaluate the configuration using the algorithm outlined above in order to obtain the comparisons presented in Fig. 21. It can clearly be seen that the automated configuration sorting algorithm provides very good comparisons for the calculated probabilities of occurrence for different configuration classes, as long as they are compared at the same level of coarse graining.

References

Al-Mubaiyedh, U. A., R. Sureshkumar, and B. Khomami, "Linear stability of viscoelastic taylor-couette flow: Influence of fluid rheology and energetics," J. Rheol. **44**, 1121–1138 (2000).

Arora, K., and R. Sureshkumar, "A viscoelastic flow instability near the solid body rotation limit," J. Non-Newtonian Fluid Mech. **132**, 36–44 (2005).

Babcock, H. P., D. E. Smith, J. S. Hur, E. S. G. Shaqfeh, and S. Chu, "Relating the microscopic and macroscopic response of a polymeric fluid in a shearing flow," Phys. Rev. Lett. **85**, 2018–2021 (2000).

Babcock, H. P., R. E. Teixeria, J. S. Hur, E. S. G. Shqfeh, and S. Chu, "Visualization of molecular fluctuations near the critical point of the coil-stretch transition in polymer elongation," Macromolecules **36**, 4544–4548 (2003).

Bird, R. B., C. F. Curtiss, R. C. Armstrong, and O. Hassager, *Dynamics of Polymeric Liquids, Vol I* (Wiley, New

York, 1987a).

Bird, R. B., C. F. Curtiss, R. C. Armstrong, and O. Hassager, *Dynamics of Polymeric Liquids, Vol II* (Wiley, New York, 1987b).

de Gennes, P. G., "Coil-stretch transition of dilute flexible polymers under ultrahigh velocity gradients," J. Chem. Phys. **60**, 5030–5042 (1974).

Doyle, P. S., B. Ladoux, and J. L. Viovy, "Dynamics of tethered polymer in shear flow," Phys. Rev. Lett. **84**, 4769–4772 (2000).

Doyle, P. S., E. S. G. Shaqfeh, and A. P. Gast, "Dynamic simulation of freely draining flexible polymers in steady linear flows," J. Fluid Mech. **334**, 251–291 (1997).

Doyle, P. S., E. S. G. Shaqfeh, G. H. McKinley, and S. H. Spiegelberg, "Relaxation of dilute polymer solutions following extensional flow," J. Non-Newtonian Fluid Mech. **76**, 79–110 (1998).

Ghosh, I., Y. L. Joo, G. H. McKinley, R. A. Brown, and R. C. Armstrong, "A new model for dilute polymer solutions in flows with strong extensional components," J. Rheol. **46**, 1057–1089 (2002).

Gigras, P. G., and B. Khomami, "Adaptive configuration fields: A new multiscale simulation technique for reptation based models with a stochastic strain measure and local variations of life span distribution," J. Non-Newtonian Fluid Mech. **108**, 99–122 (2002).

Gupta, V. K., R. Sureshkumar, and B. Khomami, "Polymer chain dynamics in newtonian and viscoelastic turbulent channel flows," Phys. Fluids **16**, 1546–1566 (2004).

Halin, P., G. Lielens, R. Keunings, and V. Legat, "The Lagrangian particle method for macroscopic micro-macro viscoelastic flow computations," J. Non-Newtonian Fluid Mech. **79**, 387–403 (1998).

Herrchen, M., and H. C. Öttinger, "A detailed comparison of various FENE dumbbell models," J. Non-Newtonian Fluid Mech. **68**, 17–42 (1997).

Hua, C. C., J. D. Schieber, and D. C. Venerus, "Segment connectivity, chain-length breathing, segmental stretch and constraint release in reptation models. III. Shear flows," J. Rheol. **43**, 710–717 (1999).

Hulsen, M. A., A. P. G. van Heel, and B. H. A. A. van den Brule, "Simulation of viscoelastic flows using Brownian configuration fields," J. Non-Newtonian Fluid Mech. **70**, 79–101 (1997).

Hur, J. S., E. S. G. Shaqfeh, and R. G. Larson, "Brownian dynamics simulations of single DNA molecules in shear flow," J. Rheol. **44**, 713–742 (2000).

Keunings, R., "On the Peterlin approximation for finitely extensible dumbbells," J. Non-Newtonian Fluid Mech. **68**, 85–100 (1997).

Keunings, R., "Micro-macro methods for the multiscale simulation of viscoelastic flow using molecular models of kinetic theory," Rheology Reviews, 2004.

Koppol, A. P., R. Sureshkumar, and B. Khomami, "An efficient algorithm for multiscale flow simulation of dilute polymeric solutions using bead-spring chains," J. Non-Newtonian Fluid Mech. **141**, 180–192 (2007).

Larson, R. G., H. Hu, D. E. Smith, and S. Chu, "Brownian dynamics simulations of a DNA molecule in an extensional field," J. Rheol. **43**, 267–304 (1999).

Larson, R. G., T. T. Perkins, D. E. Smith, and S. Chu, "Hydrodynamics of a DNA molecule in a flow field," Phys. Rev. E **55**, 1794–1797 (1997).

Laso, M., and H. C. Öttinger, "Calculation of viscoelastic flow using molecular models: The CONNFFESSIT approach," J. Non-Newtonian Fluid Mech. **47**, 1–20 (1993).

Li, C. F., R. Sureshkumar, and B. Khomami, "Influence of rheological parameters on polymer induced drag reduction," J. Non-Newtonian Fluid Mech. **140**, 23–40 (2006).

Lielens, G., P. Halin, R. Keunings, and V. Legat, "New closure approximations for the kinetic theory of finitely extensible dumbbells," J. Non-Newtonian Fluid Mech. **76**, 249–279 (1998).

Lielens, G., R. Keunings, and V. Legat, "The FENE-L and FENE-LS closure approximations to the kinetic theory of finitely extensible dumbbells," J. Non-Newtonian Fluid Mech. **87**, 179–196 (1999).

Lin, B., B. Khomami, and R. Sureshkumar, "Effect of non-normal interactions on the interfacial instability of multilayer viscoelastic channel flows," J. Non-Newtonian Fluid Mech. **116**, 407–429 (2004).

Lozinski, A., C. Chauvière, J. Fang, and R. G. Owens, "Fokker-planck simulations of fast flows of melts and concentrated polymer solutions in complex geometries," J. Rheol. **47**, 535–561 (2003).

Marko, J. F., and E. D. Siggia, "Stretching DNA," Macromolecules **28**, 8759–8770 (1995).

Öttinger, H. C., "A thermodynamically admissible reptation model for fast flows of entangled polymers," J.

Rheol. **43**, 1461–1493 (1999).

Öttinger, H. C., B. H. A. A. van den Brule, and M. A. Hulsen, "Brownian configuration fields and variance reduced CONNFFESSIT," J. Non-Newtonian Fluid Mech. **70**, 255–261 (1997).

Perkins, T. T., D. E. Smith, and S. Chu, "Single polymer dynamics in an elongational flow," Science **276**, 2016–2021 (1997).

Schroeder, C. M., H. P. Babcock, E. S. G. Shaqfeh, and S. Chu, "Observation of polymer conformation hysteresis in extensional flow," Science **301**, 1515–1519 (2003).

Schroeder, C. M., E. S. G. Shaqfeh, and S. Chu, "Effect of hydrodynamic interactions on DNA dynamics in extentional flow: Simulation and single molecule experiment," Macromolecules **37**, 9242–9256 (2004).

Sizaire, R., G. Lielens, I. Jaumain, R. Keunings, and V. Legat, "On the hysteretic behavior of dilute polymer solutions in relaxation following extensional flow," J. Non-Newtonian Fluid Mech. **82**, 233–253 (1999).

Smith, D. E., H. P. Babcock, and S. Chu, "Single-polymer dynamics in steady shear flow," Science **283**, 1724–1727 (1999).

Smith, D. E., and S. Chu, "Response of flexible polymers to a sudden elongational flow," Science **281**, 1335–1340 (1998).

Somasi, M., and B. Khomami, "Linear stability and dynamics of viscoelastic flows using time-dependent stochastic simulation techniques," J. Non-Newtonian Fluid Mech. **93**, 339–362 (2000).

Somasi, M., and B. Khomami, "A new approach for studying the hydrodynamic stability of fluids with microstructure," Phys. Fluids **13**, 1811–1814 (2001).

Somasi, M., B. Khomami, N. J. Woo, J. S. Hur, and E. S. G. Shaqfeh, "Brownian dynamics simulations of bead-rod and bead-spring chains: numerical algorithms and coarse-graining issues," J. Non-Newtonian Fluid Mech. **108**, 227–255 (2002).

Suen, J. K. C., Y. L. Joo, and R. C. Armstrong, "Molecular orientation effects in viscoelasticity," Annu. Rev. Fluid Mech. **34**, 417–444 (2002).

Sureshkumar, R., and A. N. Beris, "Linear stability analysis of viscoelastic Poiseuille flow using an Arnoldi-based orthogonalization algorithm," J. Non-Newtonian Fluid Mech. **56**, 151–182 (1995).

Teixeira, R. E., H. P. Babcock, E. S. G. Shaqfeh, and S. Chu, "Shear thinning and tumbling dynamics of single polymers in the flow-gradient plane," Macromolecules **38**, 581–592 (2005).

Underhill, P. T., and P. S. Doyle, "On the coarse-graining of polymers into bead-spring chains," J. Non-Newtonian Fluid Mech. **122**, 3–31 (2004).

Underhill, P. T., and P. S. Doyle, "Development of bead-spring models using the constant extension ensemble," J. Rheol. **49**, 963–987 (2005).

van Heel, A. P. G., M. A. Hulsen, and B. H. A. A. van den Brule, "On the selection of parameters in the FENE-P model," J. Non-Newtonian Fluid Mech. **75**, 253–271 (1998).

Venkataramani, V., R. Sureshkumar, and B. Khomami, "A computationally efficient approach for hi-fidelity fine-graining from the bead-spring models to the bead-rod models," J. Non-Newtonian Fluid Mech. **149**, 20–27 (2008).

Warner, H. R., "Kinetic theory and rheology of dilute suspensions of finitely extendible dumbbells," Ind. Eng. Chem. Fundam. **11**, 379–387 (1972).

Wedgewood, L. E., and R. B. Bird, "From molecular models to the solutions of flow problems," Ind. Eng. Chem. Res. **27**, 1313–1320 (1988).

Wedgewood, L. E., D. N. Ostrov, and R. B. Bird, "A finitely extensible bead-spring chain model for dilute polymer solutions," J. Non-Newtonian Fluid Mech. **40**, 119–139 (1991).

Wiest, J. W., and R. I. Tanner, "Rheology of bead-nonlinear spring chain macro-molecules," J. Rheol. **33**, 281–316 (1989).

Woo, N., E. S. G. Shaqfeh, and B. Khomami, "The effect of confinement on the dynamics and rheology of dilute DNA solutions. Part II: Effective rheology and single chain dynamics," J. Rheol. **48**, 299–318 (2004).

Zhou, Q., and R. Akhavan, "Cost-effective multi-mode FENE bead-spring models for dilute polymer solutions," J. Non-Newtonian Fluid Mech. **116**, 269–300 (2004).